Contents lists available at ScienceDirect

Petroleum Science

journal homepage: www.keaipublishing.com/en/journals/petroleum-science



Original Paper

Influence of gravel content and cement on conglomerate fracture

Zhen-Xin Zhang $^{\rm a}$, Hong-Kui Ge $^{\rm a,\,*}$, Jian-Bo Wang $^{\rm b}$, Jian-Tong Liu $^{\rm a}$, Dun-Qing Liu $^{\rm b}$, Wei-Wei Teng ^c, Ying-Hao Shen ^a



^b Department of Petroleum Engineering, China University of Petroleum (Beijing) at Karamay, Karamay, 834000, Xinjiang, China

ARTICLE INFO

Article history: Received 24 February 2022 Received in revised form 26 March 2023 Accepted 27 March 2023 Available online 31 March 2023

Edited by Yan-Hua Sun

Keywords: Conglomerate Mechanical property Fracture characteristics Crack evolution

ABSTRACT

Tight reservoirs are typically developed by horizontal wells and multi-stage hydraulic fracturing. The conglomerate reservoir is one type of tight reservoirs, which is different from homogeneous rock, such as tight sandstone. This is because that the existence of gravels makes conglomerate have strong heterogeneity. Thus, it is difficult to grasp the fracture mechanism and the law of fracture propagation of conglomerate, which limits the efficient development of the conglomerate reservoir. In this paper, the fracture characteristics and factors influencing the fracturing of Mahu conglomerate were studied by uniaxial compression, acoustic emission monitoring and X-ray computed tomography (CT) scanning experiments. The results show that the fracture characteristics of conglomerates are influenced by the gravel content and cement. The conglomerate in the study area is mainly divided into carbonate cemented conglomerate and clay cemented conglomerate. The fracture complexity of carbonate cemented conglomerate first increases and then decreases with increasing gravel content. However, for clay cemented conglomerates, the fracture complexity increases over the gravel content. The crack development stress is a significant parameter in the crack assessment of conglomerates. This study is useful to understand the influence of meso-fabric characteristics of conglomerates on their fracturing and crack evolution and guides the design of hydraulic fracturing.

© 2023 The Authors. Publishing services by Elsevier B.V. on behalf of KeAi Communications Co. Ltd. This is an open access article under the CC BY-NC-ND license (http://creativecommons.org/licenses/by-nc-nd/

4.0/).

1. Introduction

Conglomerate reservoirs are widely distributed in China, the United States, Canada, Brazil, Australia, and other countries (Cronin and Kidd, 1998; Hentz et al., 2012; Arnott, 2003; Macquaker et al., 2014). The geological reserves of conglomerate reservoirs discovered in the Junggar Basin of Xinjiang, China, exceed 1 billion tons (Hou et al., 2018; Jia et al., 2018). However, the sedimentary environment of conglomerate reservoirs has characteristics of low porosity and low permeability (Jia et al., 2017). Thus, hydraulic fracturing is generally used as an essential method to develop conglomerate reservoirs. Since the conglomerate has strong heterogeneity, the tortuous and complex hydraulic fractures formed during fracturing make it difficult to evaluate the reconstruction effect (Xv et al., 2019), restricting the fracturing construction

Corresponding author. E-mail address: gehongkui@163.com (H.-K. Ge).

design. Therefore, it is necessary to study the propagation law of conglomerate fractures.

In recent years, some scholars have studied the propagation mechanism of conglomerate fractures using experiments and numerical simulations. True triaxial hydraulic fracturing experiments were conducted on artificial and natural conglomerate specimens (Meng et al., 2010; Ma X. et al., 2017; Xv et al., 2019; Ma D. et al., 2020). These studies observed that gravel-deflecting, gravel-penetrating, branching, arresting, and terminating would occur when hydraulic fractures intersect with gravels in the process of fracture propagation. Numerical simulations of conglomerate hydraulic fracturing were performed by using finite element and discrete element methods based on fracture mechanics and damage mechanics theory (Liu et al., 2016; Rui et al., 2018; Li et al., 2013). It has found that the complexity of fractures was significantly related to gravel particle size and content. Preliminary studies were made on the mechanical properties of conglomerate by triaxial compression tests and direct shear tests (Liu et al., 2018; He et al., 2019; Zhu J. et al., 2019). The result shows that gravels have a great influence

^c CNPC Xinjiang Oilfield Company, Karamay, 834000, Xinjiang, China

on the compressive, shear, and tensile strength of conglomerate. Particle flow discrete element numerical simulation was used to simulate the uniaxial compression experiment of conglomerate and explore the effect of gravel content on mechanical properties of the conglomerate (Luo et al., 2021). Three-point bending test was conducted on semi-circular specimens and found that conglomerate can be divided into gravel-enhanced conglomerate and gravel-weakened conglomerate (Liu et al., 2022).

The previous studies reveal the main controlling factors of the mechanical properties of conglomerate and the regularity of fracture propagation. But the research on the conglomerate fracture morphology only considers the influence of gravels. Either the impact of cement or the influence of crack evolution on fracturing characteristics before conglomerate failure is not considered. Studying crack evolution characteristics before conglomerate failure and fracture morphology after failure is conducive to revealing the fracture mechanism of the conglomerate.

The characteristics of crack evolution and fracture morphology of homogeneous rocks have been widely studied. Scholars found that before rock is destroyed, cracks and other defects would suffer from an evolutionary process of initiation, development, propagation, and coalescence (Griffith, 1921; Erarslan, 2013). The evolution of cracks was characterized by introducing the volume strain of cracks and the evolution process of cracks was divided into five stages, namely, crack closure stage, elastic stage, stable crack stage, unstable cracking stage, and post-peak deformation stage (Martin and Chandler, 1994). The traditional triaxial compression experiment is a simple method to study the evolution of cracks, but it has limitations in studying the microscopic fracture in crack evolution. For this reason, acoustic emission is used to monitor the fracture events in rock (Pestman and van Munster, 1996; Wang et al., 2021a). X-ray computed tomography (CT) scanning technology is used to visually characterize rock fractures (Cnudde et al., 2011; Jia et al., 2013; Zhang Y. et al., 2020).

This article takes the Mahu conglomerate as an example and obtains two types of conglomerates with different cementation. Uniaxial compression, acoustic emission monitoring, and CT scanning experiments are used to study the fracture characteristics and crack evolution of conglomerate. The fracture characteristics and factors influencing the fracturing of conglomerate are investigated. The influence of cementation type and gravel content on crack evolution, fracture morphology and fracture complexity are studied. Fractal dimension analysis and Sholl analysis are introduced to quantitatively characterize the tortuosity degree and distribution density of fractures.

2. Specimens and experimental methods

2.1. Experimental specimens

Conglomerate specimens were taken from the Triassic Baikouquan Formation and the Upper Permian Wuerhe Formation in Mahu sag, Junggar Basin, Xinjiang. The buried depth of the Baikouquan Formation is 3708—3719 m, and that of the Upper Wuerhe Formation is 3599—3704 m. The specimens for the uniaxial compressive strength test have a diameter of 38 mm and a height of 76 mm. Specimens from Baikouquan Formation were numbered as group Z, and specimens from Wuerhe Formation were numbered as X. Each group of conglomerates contained 5 specimens. The specimen photos are shown in Fig. 1 and the detailed information of the specimens is shown in Table 1.

The gravel content of the experimental specimens was calculated by image processing (Fig. 2). Firstly, the image of the specimen surface was captured, and then the contour of the gravel in the image was extracted. Finally, the gravel area was calculated by

image processing software, and the gravel content was the ratio of the extracted gravel area to the overall surface area of the specimens (Luo et al., 2021; Liu et al., 2022).

Fig. 3 shows the X-ray fluorescence (XRF) element maps of conglomerate specimens from group Z (the Baikouquan Formation) and group X (the Wuerhe Formation), showing the contents and distribution of Al, Ca, Fe, Mg, Si, K, Mn, and Na in the specimens. Fig. 4(a) and (b) are scanning electron microscope (SEM) and energy dispersive spectroscopy (EDS) maps of group Z. Fig. 4(c) and (d) are SEM and EDS of specimens in group X respectively. It can be seen that the cement of conglomerate specimens in group X mainly contain Al and Si and a little Ca and Mn, while the cement of group Z mainly consists of Fe and Mn. According to the study of conglomerate cement, the main types of cement in conglomerate include carbonate cement mainly composed of calcite and siderite, and aluminosilicate cement mainly composed of clay (Zhu N. et al., 2019; Wang et al., 2021b; Xi et al., 2021). In this study, the cement type of specimens in group Z is mainly carbonate cement, while that of specimens in group X is mainly clay cement.

2.2. Experimental methods

2.2.1. Uniaxial compression and acoustic emission monitoring

The experimental instrument used in the uniaxial compression experiment, the RTR-1000 triaxial mechanical test system from the GCTS company, was shown in Fig. 5(b), with a maximum axial pressure of 1000 kN, a displacement resolution of 0.1 µm, a load resolution of 0.01 kN, and a sampling frequency of 10 Hz. Before the experiment, specimens were sent to a specimen storage room. where the specimens were stored at constant temperature $(25 \pm 1 \, ^{\circ}\text{C})$ and constant humidity $(30\% \pm 1\%)$ for more than 30 days. Specimens were treated at 50 °C until its weight is not reduced in order to fully dry the specimens and prevent the specimens from thermal cracking. Then the specimens were removed and their sizes (diameter and height) were measured. The specimen was put into the test instrument and then covered with a heat-shrinkable tube to ensure that it can remain intact after the experiment. The uniaxial compression test was loaded at an axial strain rate of 0.05%/min in strain rate mode until failure. The axial force and displacement were automatically monitored by sensors.

During the uniaxial compression experiment, acoustic emission events were monitored by the Richter Data Acquisition and Streaming System from Itasca. The response frequency of the acoustic emission sensor is 1 MHz, and the noise threshold is 70 dB, as shown in Fig. 5(c). The acoustic emission probe was pasted 20 mm away from the top of the specimen, and the installed experimental specimen is as shown in Fig. 5(a).

2.2.2. CT scan

After the uniaxial compression test, the experimental specimen was removed and put into a CT scanner for scanning. The instrument used for CT scanning is Nano Voxel 30502E, with a spatial resolution ranging from 3 to 30 µm, the diameter of scannable specimens ranging from 5 to 300 mm, the maximum tube voltage of X-ray source being 160 kV, and the maximum power being 10 W, as shown in Fig. 5(d). The scanning range is 28.78 mm in diameter and 23.0 mm in height, and the scanning resolution ratio is 14.99 µm. The image generated by CT scan is affected by many factors, which would produce a series of noises and image artifacts. These artifacts and noises reduce the image quality and are not conducive to subsequent quantitative analysis. A median filtering method was adopted to de-noise the image so as to optimize the image quality. In this article, a 5×5 rectangle is used as the window of median filtering, and the gray value of each pixel is set as the median of the gray value of all pixels in a neighboring window of

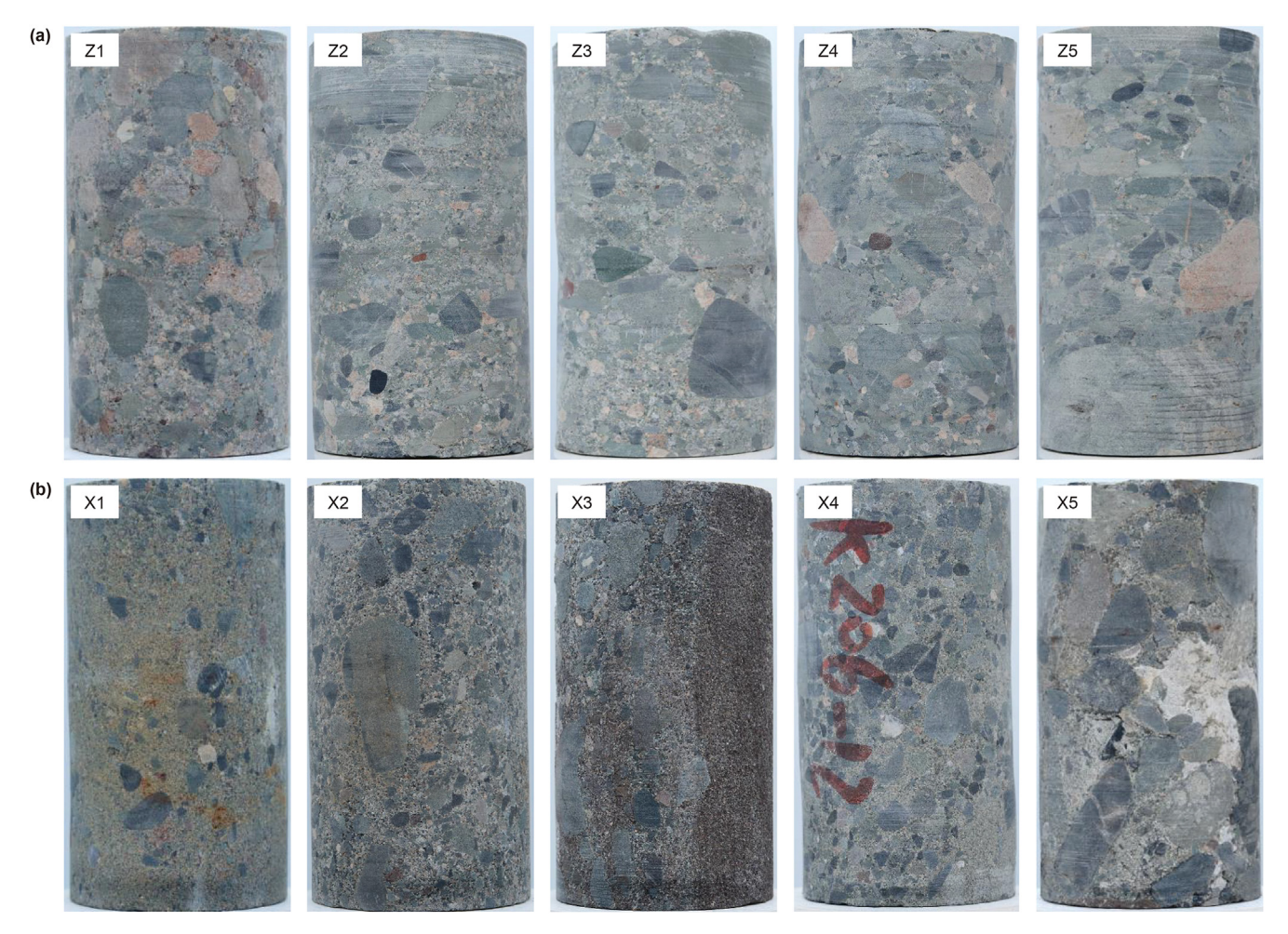


Fig. 1. Images of specimens before experiment.

Table 1Basic data of experimental specimens.

Specimen No.	Gravel content, vol%	Diameter, mm	Height, mm	Porosity, %
Z1	25.5	38.25	77.14	7.76
Z2	30.8	38.20	77.38	8.92
Z3	41.2	38.14	76.39	7.05
Z4	55.4	38.30	77.26	10.18
Z5	60.3	38.04	76.63	9.66
X1	10.4	38.15	71.13	7.35
X2	14.6	38.10	78.13	11.00
X3	25.8	38.27	76.44	8.05
X4	35.6	38.32	78.93	7.36
X5	63.3	38.14	76.93	7.76

the point. After processing, the transition zone between fractures and rock particles became natural and smooth, and most of the noise, illusion, and some isolated pores were removed. The images before and after the median filtering are as shown in Fig. 6.

3. Experimental results

3.1. Mechanical properties

Fig. 7 shows stress—strain curves of two groups of conglomerate specimens with different gravel contents. It can be seen from the stress—strain curve that the specimens from the Baikouquan Formation (Group Z) suffer from a brittle failure, and multiple

fracturing happened before the load reaches the peak strength. While specimens of the Upper Wuerhe Formation (group X) are mainly plastic failures, and the phenomenon of multiple fractures is rare.

Table 2 shows the compressive strength, elastic modulus, and Poisson's ratio of conglomerate specimens. For specimens in group Z, the uniaxial compressive strength (UCS) ranges from 26.4 to 60.4 MPa with an average of 45.3 MPa, and the elastic modulus (E) ranges from 18.1 to 25.8 GPa with an average of 21.4 GPa. The specimens in group X have a uniaxial compressive strength ranging from 22.5 to 57.4 MPa with an average of 36.9 MPa, and an elastic modulus ranging from 9.8 to 23.1 GPa with an average of 14.8 GPa. The compressive strength and elastic modulus of specimens in group Z are higher than those in group X. Comparing with the previous experiments, where the elastic modulus of rock samples ranged from 29.01 to 78.15 GPa, with an average of 48.04 GPa, the Poisson's ratio is 0.15-0.75, with an average of 0.37, and the uniaxial compressive strength is 14.0-54.5 MPa, with an average of 36.5 MPa (Liu et al., 2018), it can be seeing that the conglomerate is highly heterogeneous and its mechanical properties vary greatly in different strata and regions.

3.2. Fracture characteristics

3.2.1. Morphological characteristics of fractures

Based on CT scanning, the fractures formed in specimens in group Z and group X after the uniaxial compression experiment

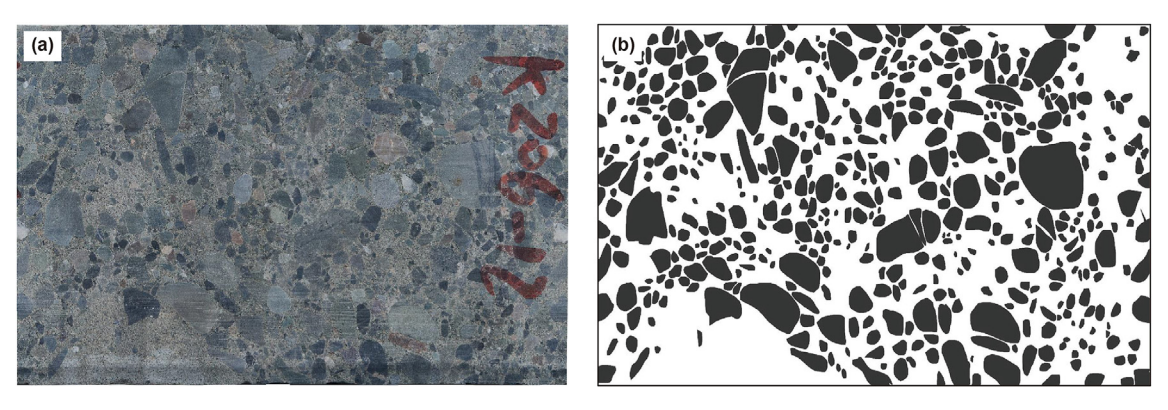


Fig. 2. Extracted gravel contour and the calculation of gravel content. (a) The cylindrical surface of specimen; (b) The extracted gravel contour image.

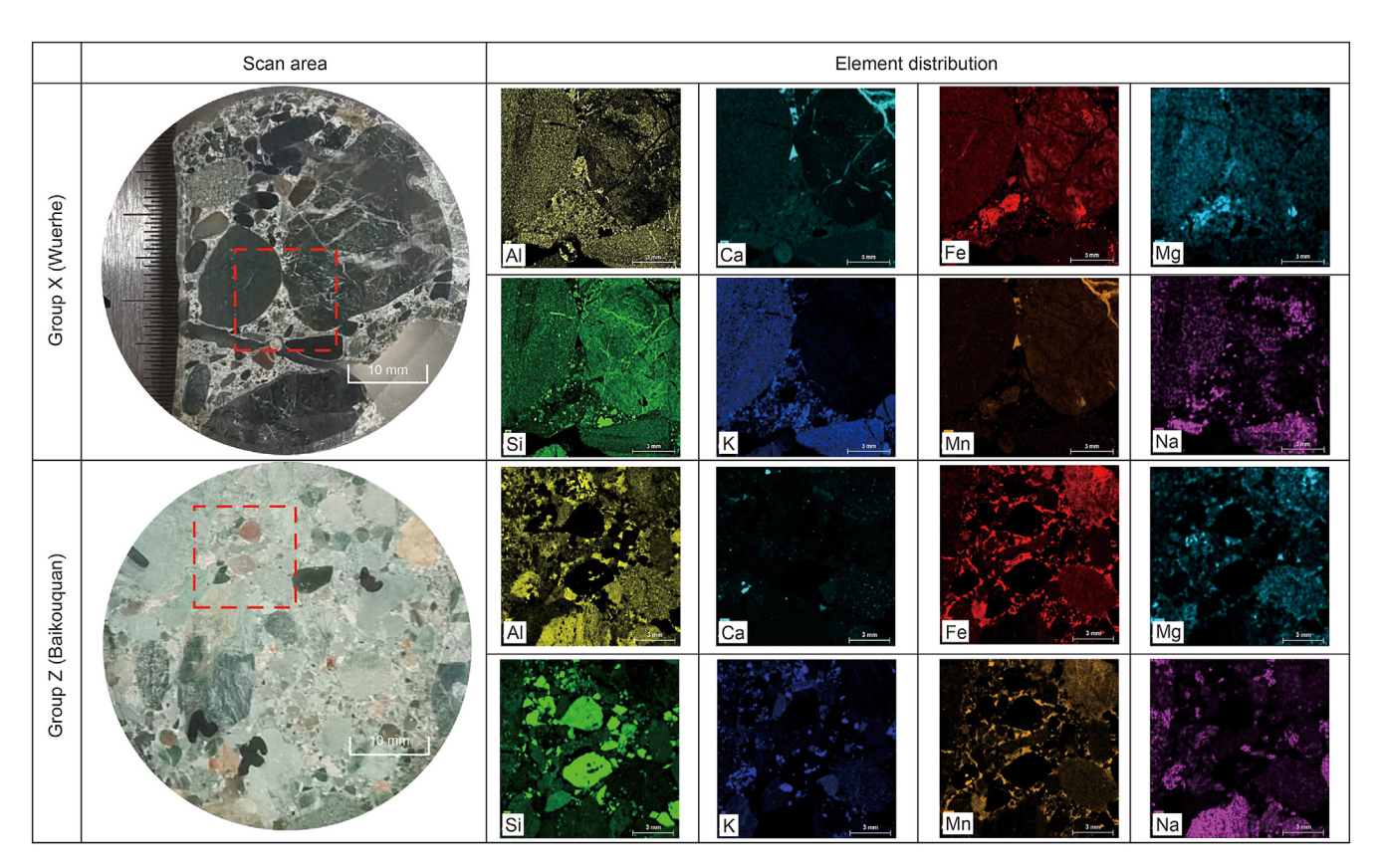


Fig. 3. The X-ray fluorescence (XRF) elemental maps showing the distribution and content of Al, Ca, Fe, Mg, Si and K in the group Z and group X.

were extracted to analyze the morphological characteristics and influencing factors of the fracture. The scanning scope is a cylindrical area with a diameter of 28.8 mm and a height of 23.0 mm. Fig. 8 shows the steps of CT reconstruction. Fig. 8(a) shows the range of CT scan, Fig. 8(b) shows the 3D reconstructed specimen images, and Fig. 8(c) shows the extracted fracture image.

The CT reconstruction image of group Z is as shown in Fig. 9. It can be seen that when the gravel content of group Z is low (Z1, 25.5 vol% of gravel content), the fractures formed in group Z are relatively simple, with obvious main fractures and undeveloped branch fractures. Meanwhile, it is observed that the fractures would surround gravels when they encounter gravels. As the gravel content increases (Z2, 30.8 vol% of gravel content), two obviously intersecting fractures are formed accompanied by undeveloped branch fractures. When the fractures encounter gravel, although a

little would penetrate through gravel, mainly of them remain to surround gravel. As the gravel content further increases (Z3, 41.2 vol% of gravel content), a complex fracture network is formed with no obvious main fractures. The gravel-surrounding fractures develop together with the gravel-penetrating fractures. When the gravel content is much higher (Z5, 60.3 vol% of gravel content), the fractures formed are relatively simple with obvious main fractures and extend through the gravels.

Fig. 10 shows the CT reconstruction of the specimens in group X. When the gravel content of the specimens in group X is low (X1, 10.4 vol% of gravel content; X2, 14.6 vol% of gravel content), the fractures formed are relatively simple, with obvious main fractures and undeveloped branch fractures. With the increase of gravel content (X3, 25.8 vol% of gravel content; X4, 35.6 vol% of gravel content; X5, 63.3 vol% of gravel content), the fracture morphology

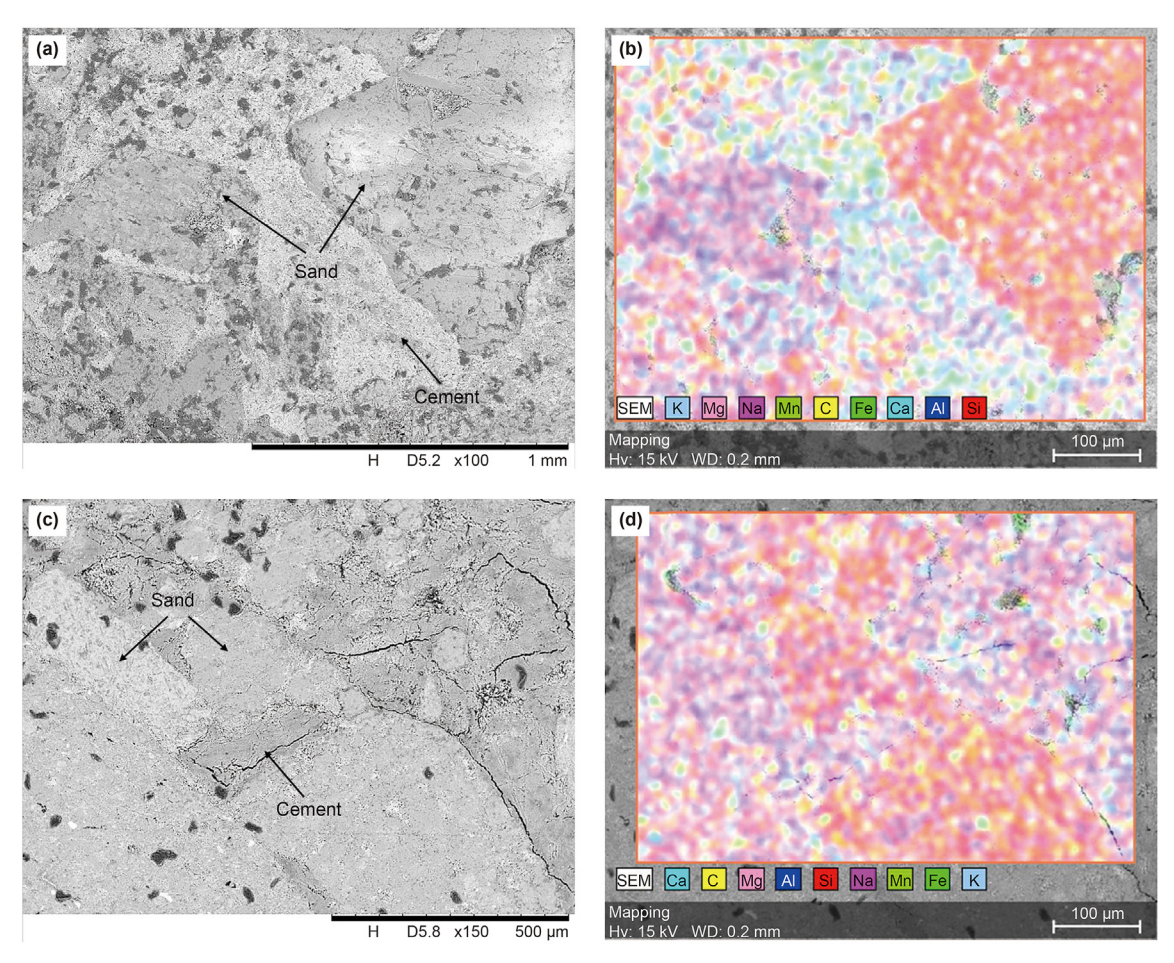


Fig. 4. The SEM (a, c) and EDS (b, d) maps of conglomerate specimens from group Z (a, b) and group X (c, d).

is more and more complex, accompanied by more branch fractures. Meanwhile, the main fractures are not obvious anymore, and the gravel-surrounding fractures develop together with the gravel-penetrating fractures, but the fractures mainly surround gravels.

3.2.2. Characterization of fracture complexity

The complexity of fractures is divided into tortuosity of single fracture and distribution density of branch fractures. To characterize the complexity of fractures, the fractal dimension method and the Sholl method are used to characterize the tortuosity of a single fracture and the distribution density of branch fractures, respectively. The fractal dimension can characterize the irregular morphology and tortuosity of the fracture surface. The larger the fractal dimension of the fracture is, the larger the tortuosity of the fracture is and the more irregular the fracture surface is (Tatone and Grasselli, 2015; Ju et al., 2014). There are many definitions of the fractal dimension, such as the Hausdorff dimension, the Lyapunov dimension, and box-counting dimension. The box-counting dimension has become one of the effective methods to calculate fractal dimension because of its simple calculation. Box-counting fractal dimension is obtained by calculating the number of grids in different sizes occupied by graphs and then by linear regression (Falconer, 2014; Peitgen et al., 2004).

$$dim_{box}(S) = \lim_{n \to 0} \frac{lgN(S)}{-lgn}$$
 (1)

where $\dim_{\text{box}}(S)$ represents the fractal dimension of graph S; N(S)

represents the number of grids occupied by graph S; and n represents the length of the grid. Based on the above principle, the three-dimensional fractal dimension of fractures in specimens was determined by Avizo software. The fractal dimension of fractures is as shown in Table 2.

To characterize the distribution density of branch fractures, the Sholl method, which is used for quantitative analysis of axons and dendrites of neurons in medicine, is used to analyze the distribution density of branch fractures. The principle of Sholl method is to superimpose a group of concentric circles on neurons and obtain the branching patterns of dendrites and axons of neurons in different regions by calculating the number of branches intersecting each circle, thus quantitatively characterizing the morphological characteristics of neurons (Sholl, 1953; Ferreira et al., 2014).

Fig. 11 shows the analysis process of the Sholl method. Firstly, CT images to be processed are selected and fractures are extracted by threshold segmentation. The size of the CT scanning range is circular with a diameter of 28.78 mm. Since fractures formed by uniaxial compression have no obvious fracture initiation center, the center of the CT image is taken as the center of the circle for the Sholl analysis. In addition, 0.225 mm is taken as the radius of each increase of the concentric circles to count the number of intersection points formed by fractures together with concentric circles. Then the average number of intersection points of all the concentric circles is calculated. This average is called the intersection index to characterize the distribution density of branch fractures. To eliminate statistical contingency, 10 CT images were taken from each specimen isometrically for analysis, with an interval of 2.88 mm

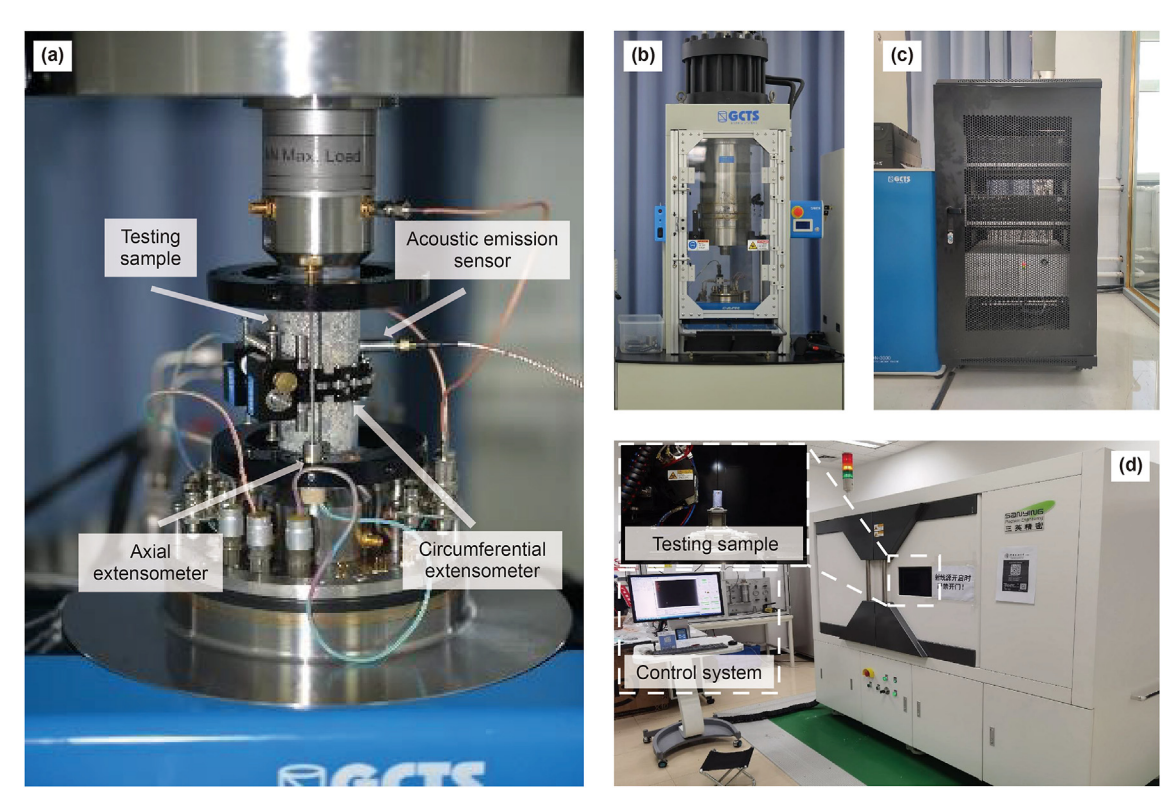


Fig. 5. Experimental instruments. (a) An installed experimental specimen; (b) RTR-1000 for uniaxial compression test; (c) The Richter Data Acquisition and Streaming System of Itasca; (d) Nano Voxel 30502E CT scanning instrument.

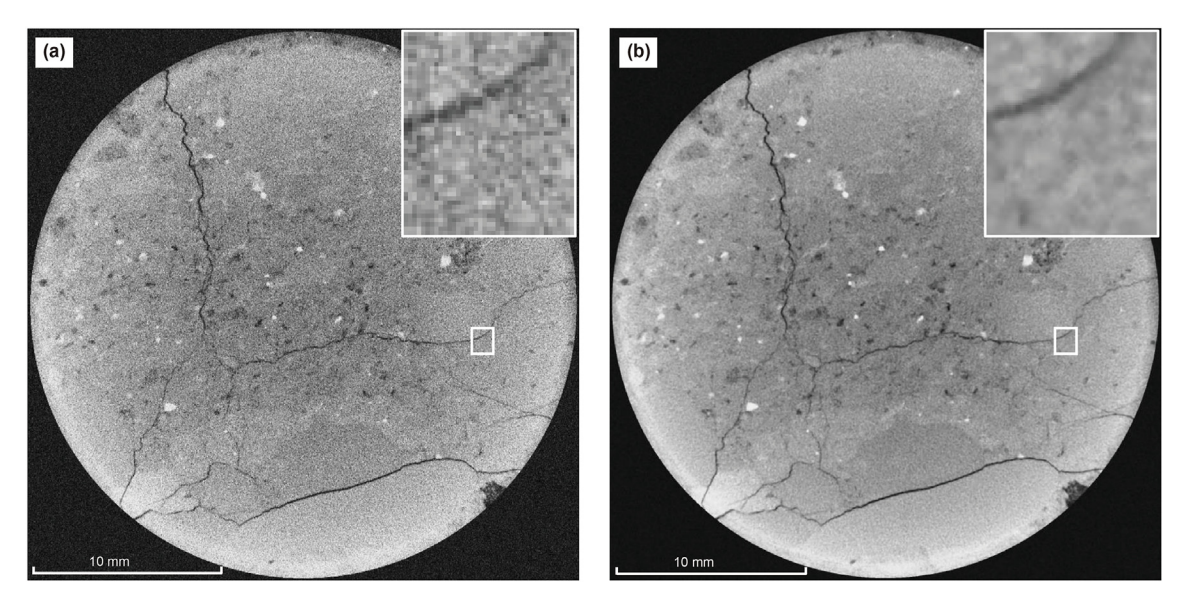


Fig. 6. Median filtering figure. (a) Original figure before median filtering; (b) Figure after median filtering.

between two successive images. The arithmetic average of the number of intersection points of 10 images is calculated as a parameter (i.e., the intersection index) to quantitatively characterize fracture distribution density.

Table 3 shows the fractal dimension and intersection index of specimens in group Z and group X. For specimens in group Z, the fractal dimension ranges from 2.097 to 2.295, with an average of 2.188 and the intersection index ranges from 4.15 to 10.5, with an average of 7.076. As to specimens in group X, the fractal dimension

ranges from 2.126 to 2.358, with an average of 2.215 and the intersection index ranges from 3.50 to 11.6, with an average of 5.77.

3.3. Evolution characteristics of conglomerate cracks

During the uniaxial compression experiment, the properties of rock would change due to the evolution of its internal cracks. AE can be used to monitor the generation and evolution of cracks in uniaxial compression experiments, and the volumetric strain of

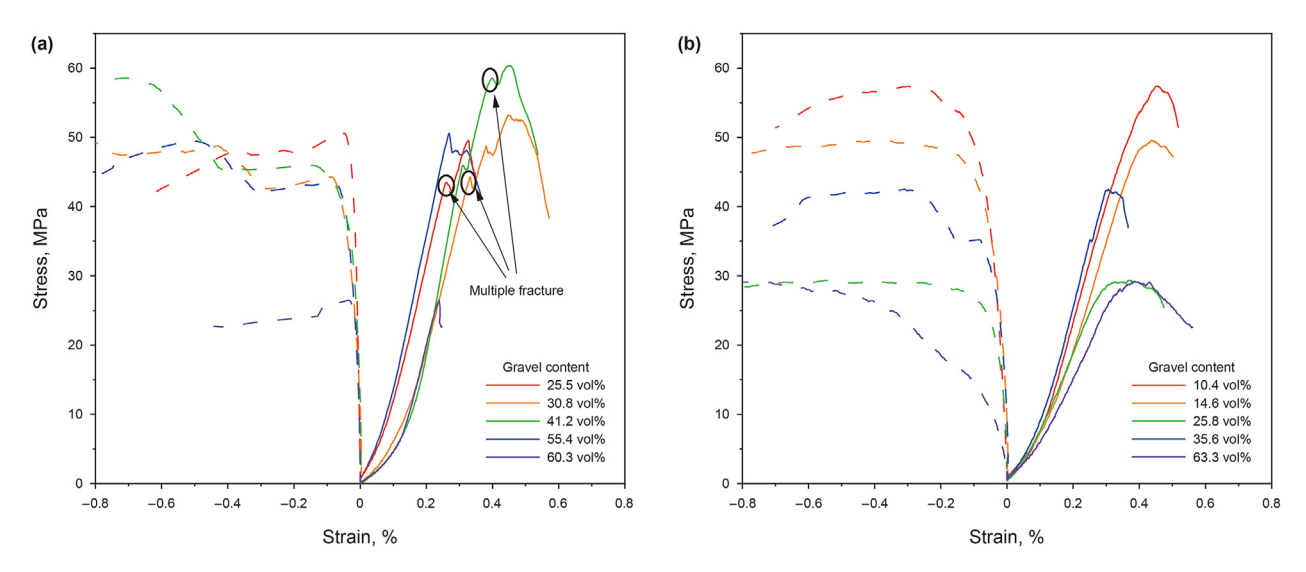


Fig. 7. Stress-strain curves of two groups of conglomerate specimens. (a) Baikouquan group specimens (Group Z); (b) Upper Wuerhe group specimens (group X).

Table 2Basic data and mechanical properties of experimental specimens.

basic data and incentinual properties of experimental specimens.					
Specimen No.	Gravel content, vol%	Uniaxial compressive strength, MPa	Elastic modulus E, GPa	Poisson's ratio	
Z1	25.5	49.5	18.9	0.17	
Z2	30.8	53.2	18.4	0.20	
Z3	41.2	60.4	25.8	0.24	
Z4	55.4	50.5	22.3	0.09	
Z5	60.3	26.4	18.1	0.09	
X1	10.4	57.4	17.8	0.22	
X2	14.6	49.6	14.7	0.23	
X3	25.8	29.4	11.3	0.22	
X4	35.6	42.5	19.9	0.30	
X5	63.3	29.2	9.8	0.48	

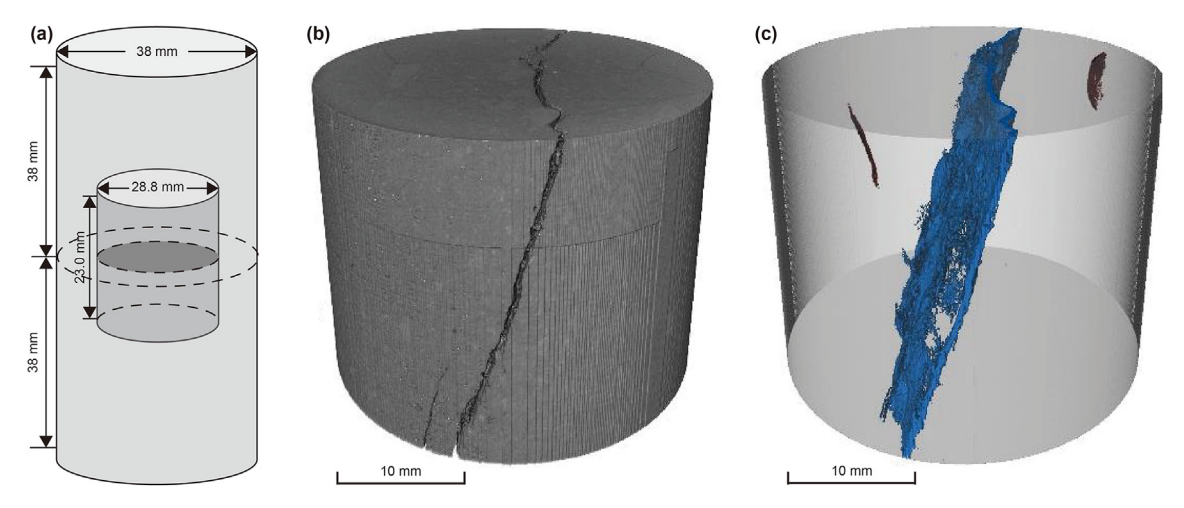


Fig. 8. The steps of 3D reconstruction. (a) Range and location of CT scan; (b) Reconstructed specimen image; (c) Extracted fracture image.

crack can be used to characterize the evolution degree of cracks.

The volumetric strain of crack can be obtained by subtracting the elastic volumetric strain from the total volumetric strain (Martin and Chandler, 1994):

$$\varepsilon_{\rm C} = \varepsilon_{\rm V} - \varepsilon_{\rm e}$$
 (2)

where $\varepsilon_{\rm C}$ is the volumetric strain of crack; $\varepsilon_{\rm V}$ is the total volumetric strain; $\varepsilon_{\rm C}$ is the elastic volume strain, and the total volumetric strain

 ε_{v} is:

$$\varepsilon_{\mathbf{v}} = \varepsilon_{\mathbf{a}} + 2\varepsilon_{\mathbf{l}} \tag{3}$$

where ε_a is the axial strain; ε_l is the lateral strain. The ε_a and ε_l are measured by the uniaxial compression experiment, and the elastic volume strain ε_e under uniaxial compression is

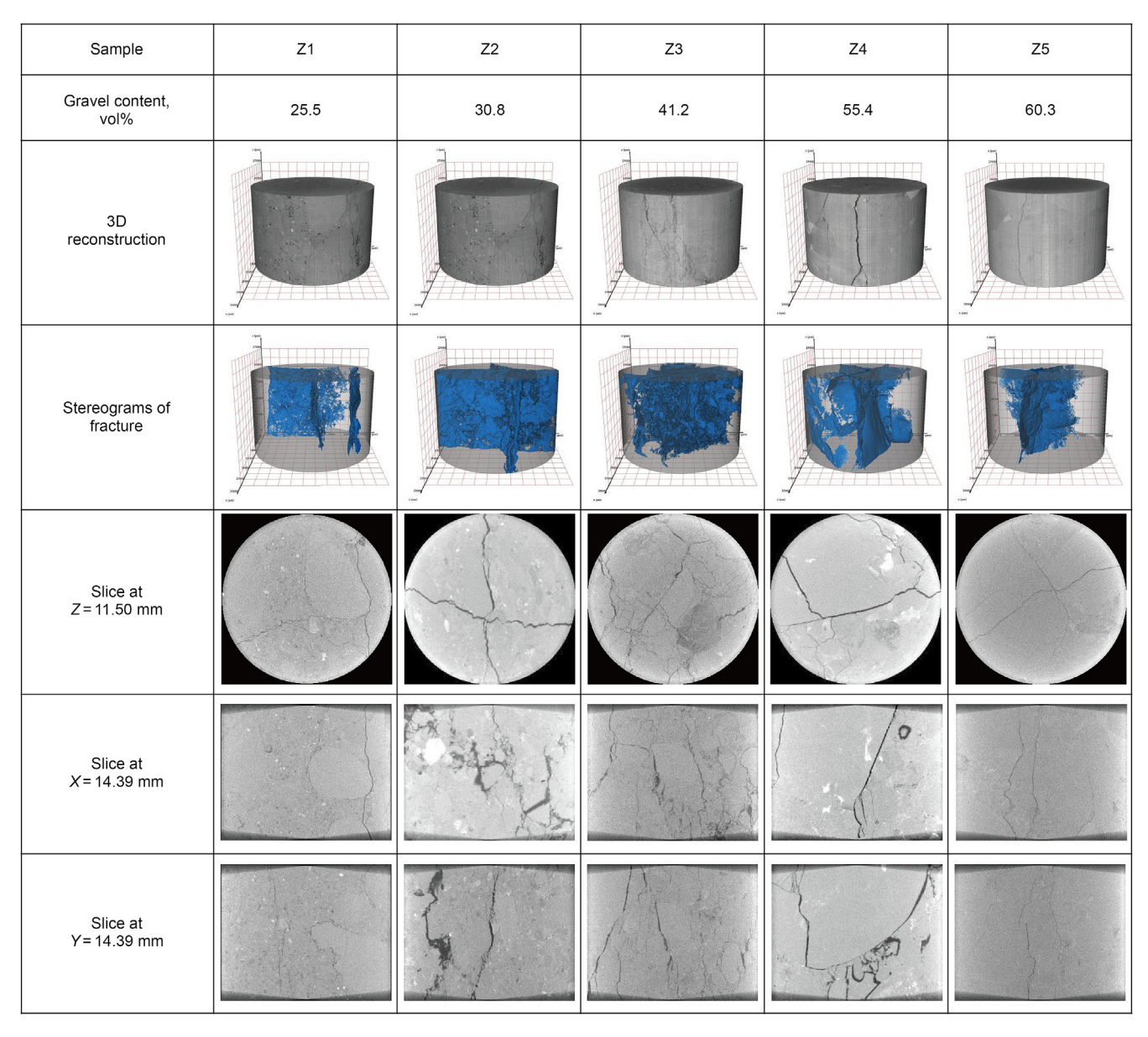


Fig. 9. 3D reconstruction images and 2D slices of three directions showing the fractures of specimens in group Z.

$$\varepsilon_{\rm e} = \frac{1 - 2\mu}{E} \sigma_{\rm a} \tag{4}$$

where μ is Poisson's ratio; E is elastic modulus.

An example of axial, lateral, and total volumetric strain versus axial stress curves, and the curve showing the relationship between AE rate and accumulative AE event number as well as axial strain for specimen X1 are given in Fig. 12. The gravel content of specimen X1 is 10.4 vol%. It can be seen that when the gravel content is low, the curve is similar to that of homogeneous brittle rock, and the evolution of crack can be divided into five stages: crack closure stage I, elastic stage II, stable crack growth stage II, unstable cracking stage IV and post-peak deformation stage V (Scholz, 1968; Brace et al., 1966; Wawersik and Brace, 1971; Tapponnier and Brace, 1976; Martin and Chandler. 1994). The crack initiation stress ($\sigma_{\rm ci}$) and the crack development stress ($\sigma_{\rm cd}$) are two important stresses in the crack evolution process. $\sigma_{\rm ci}$ is to distinguish the crack initiation stage from elastic stage, indicating the initiation of cracks in

the specimen. $\sigma_{\rm cd}$ is to distinguish the unstable cracking stage from the stable crack growth stage, which shows that the cracks inside the specimen begin to expand and eventually form macroscopic fractures

Fig. 13 shows the stress–strain curve and acoustic emission monitoring curve of conglomerate with different gravel contents in Group Z. According to Fig. 12, the crack evolution can be divided into five stages. Fig. 13(a) shows the stress–strain curve of specimen Z1 that has a gravel content of 25.5 vol%, with $\sigma_{ci}=21.46$ MPa and $\sigma_{cd}=37.94$ MPa. Multiple fracturing happened during the experiment. This phenomenon also appears in specimens Z2 and Z3, as shown in Fig. 13(b) and (c). It can be seen that the AE rate increases rapidly before first fracturing and decreases fast after fracturing. It then maintains a period of stability, in which the AE rate is at a relatively higher level than that before fracturing. Before the stress reaches its peak, the AE rate increases rapidly again. After reaching the peak stress, the stress and the AE rate decrease rapidly. Fig. 13(b) shows the stress—strain curve of specimen Z2 which has a

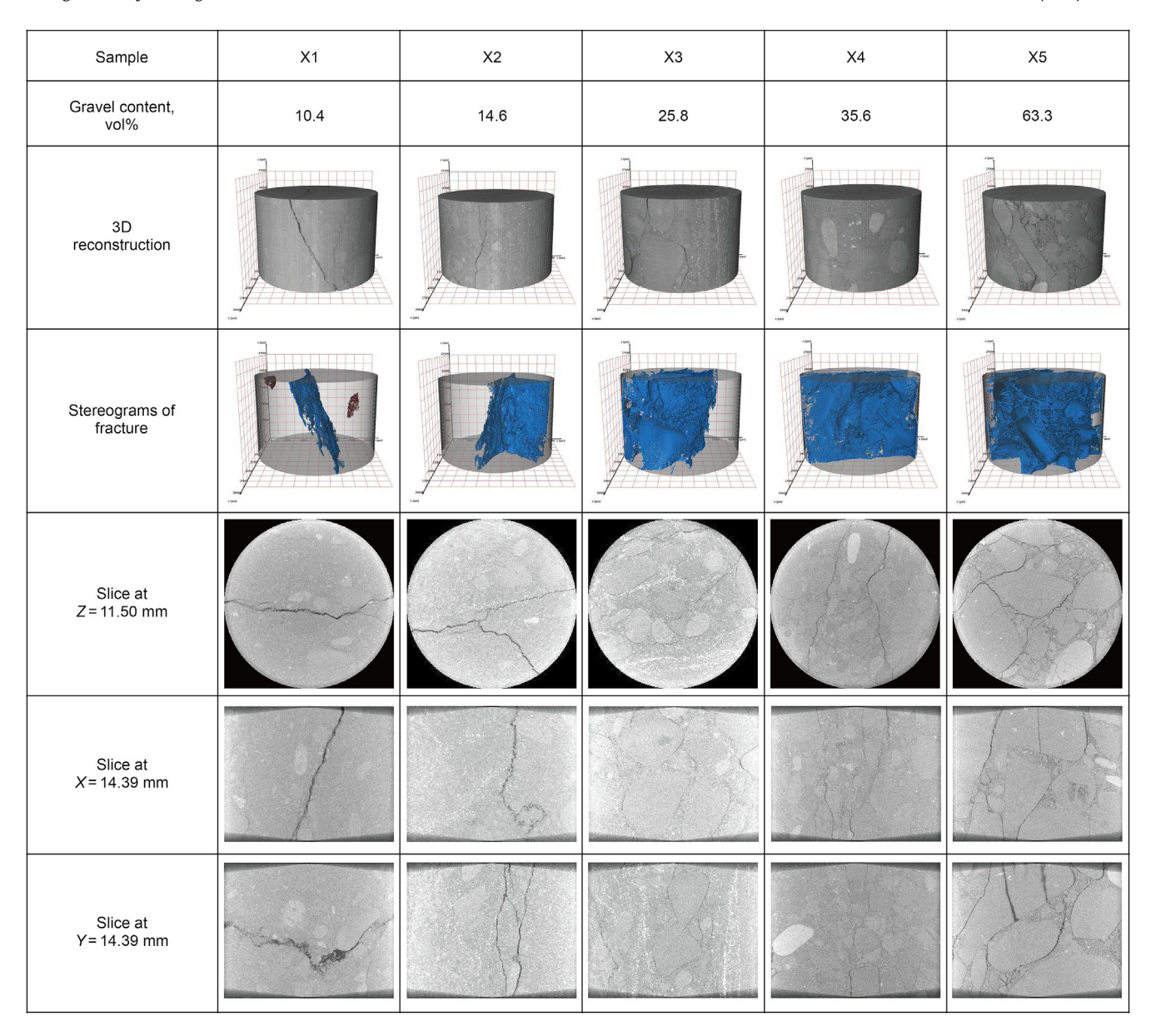


Fig. 10. 3D reconstruction images and 2D slices of three directions showing the fractures of specimens in group X.

gravel content of 30.8 vol%, with $\sigma_{ci}=24.76$ MPa and $\sigma_{cd}=32.91$ MPa. The stress does not decrease after reaching the peak stress but decreases after stabilizing for a period of time, during which the AE rate gradually increases. Fig. 13(c) shows the stress—strain curve of specimen Z3 that has a gravel content of 41.2 vol%, with $\sigma_{ci}=26.24$ MPa and $\sigma_{cd}=33.80$ MPa. Similar to specimen Z2, the AE rate events of Z3 do not decrease rapidly after peak stress, and the acoustic emission rate is maintained at 55 times/s. Fig. 13(d) shows the stress—strain curve of specimen Z5 which has a gravel content of 60.3 vol%, with $\sigma_{ci}=15.14$ MPa and $\sigma_{cd}=23.69$ MPa. It can be seen that, for Z5, no multiple fracturing happens, and the acoustic emission rate increases rapidly before peak stress and decreases rapidly after peak stress.

Fig. 14 shows the stress—strain and AE monitoring curves of conglomerate specimens with a gravel content of 10.4, 14.6, 25.8, and 63.3 vol% in group X. Fig. 14(a) shows the stress—strain diagram of specimen X1 which has a gravel content of 10.4 vol%, with $\sigma_{ci}=23.40$ MPa and $\sigma_{cd}=41.10$ MPa. The stress—strain curve and

AE characteristics of specimen X1 are similar to those of homogeneous brittle rock. At the unstable cracking stage, the AE rate increases rapidly. Then it reaches the maximum value at the peak stress and decreases rapidly at the post-peak deformation stage. Fig. 14(b) shows the stress-strain diagram of specimen X2 which has a gravel content of 14.6 vol%, with $\sigma_{ci}=26.9$ MPa and $\sigma_{cd} = 32.6$ MPa. The AE rate reaches the maximum value at the peak stress, and the AE rate at the peak is lower than that with a gravel content of 10.4 vol%. Fig. 14(c) shows the stress-strain diagram of specimen X3 that has a gravel content of 25.8 vol%, $\sigma_{ci} = 12.9$ MPa, $\sigma_{\rm cd} = 19.64$ MPa. The AE rate increases slowly in stage IV and does not have obvious peak at peak stress, but decreases slightly after peak stress. Fig. 14(d) shows the stress-strain diagram of specimen X5 that has a gravel content of 63.3 vol%, with $\sigma_{ci}=6$ MPa and $\sigma_{cd} = 7.5$ MPa. Similar to specimen X3, the acoustic emission rate rises slowly in the unstable cracking stage, and there is no obvious peak value of the acoustic emission rate at peak stress.

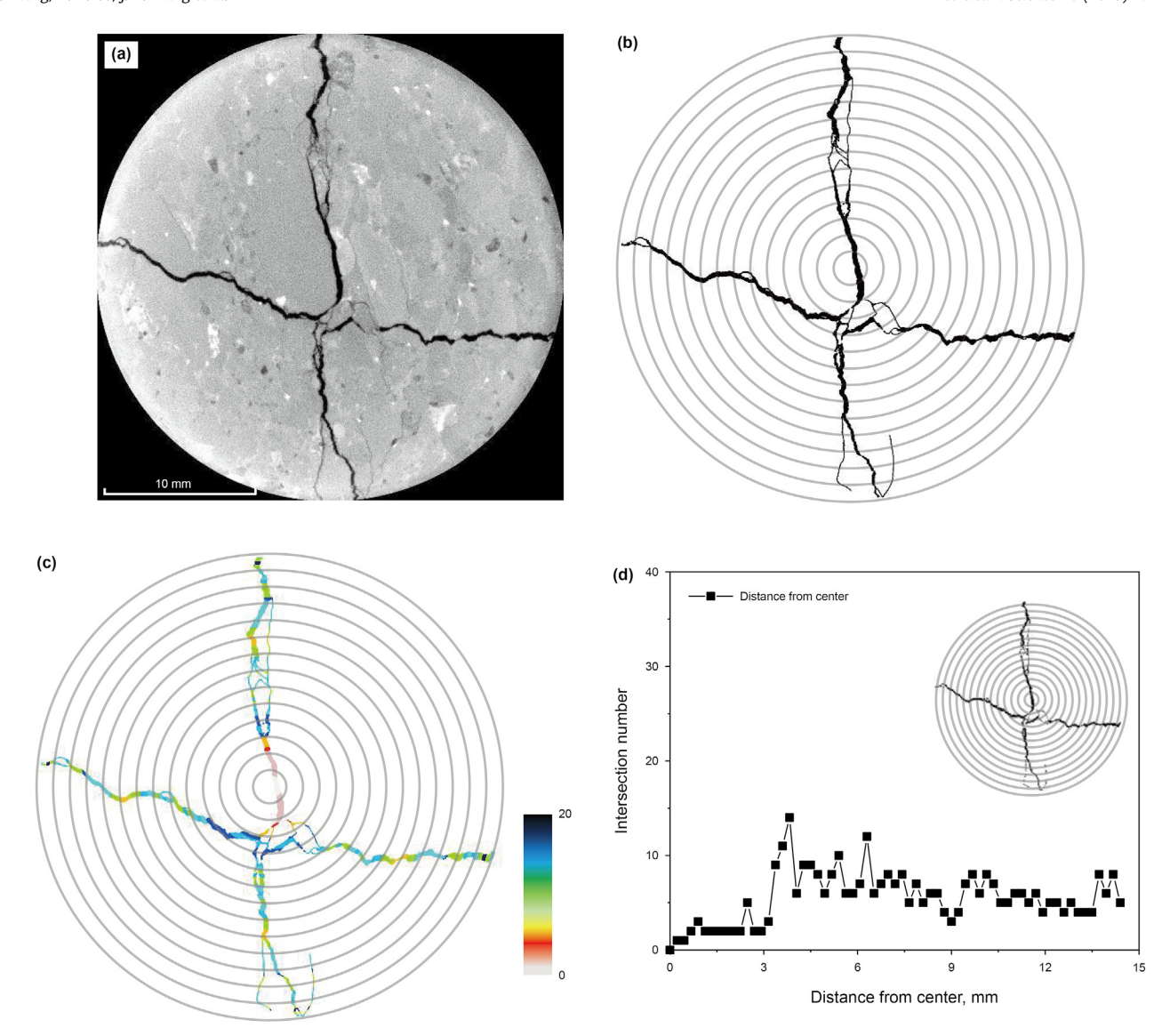


Fig. 11. The analysis process of Sholl method. (a) Original gray CT image of fracture; (b) Image of fractures and a series of concentric circles with increasing radius; (c) The number of intersection points; (d) Curve of the number of intersection points with radius.

Table 3The fractal dimension and intersection index of specimens in group Z and group X.

Specimen No.	Gravel content, vol%	Fractal dimension	Intersection index
Z1	25.5	2.097	4.51
Z2	30.8	2.260	7.06
Z3	41.2	2.295	10.5
Z4	55.4	2.114	5.98
Z5	60.3	2.175	5.33
X1	10.4	2.205	3.50
X2	14.6	2.170	3.68
X3	25.8	2.173	3.89
X4	35.6	2.126	4.68
X5	63.3	2.358	11.6

4. Discussion

4.1. Analysis of factors affecting mechanical properties

Fig. 15(a) shows the relationship between the compressive strength and gravel content of the conglomerate. When the

carbonate cemented conglomerate has a gravel content of 25.5 vol%, the uniaxial compressive strength is 49.5 MPa, and when the gravel content increases to 41.2 vol%, the uniaxial compressive strength increases to 60.4 MPa. However, as the gravel content further increases to 60.3 vol%, the uniaxial compressive strength decreases to 26.4 MPa. In the case where the clay cemented conglomerate has a gravel content of 10.4 vol%, the uniaxial compressive strength is 57.4 MPa. With the increase of gravel content, the uniaxial compressive strength gradually decreases, and when the gravel content is 63.3 vol%, the uniaxial compressive strength is 29.2 MPa. A similar pattern is also found in studies on the mechanical properties of artificial composite materials such as concrete, where the compressive strength is negatively correlated with the content of hard particles. This phenomenon ascribes to stress concentration at the edges of hard particles (Abdelaziz et al., 2018; Janeiro and Einstein, 2010). The compressive strength of carbonate cemented conglomerate is greater than that of clay cemented conglomerate under the same gravel content. The reason lies in that the cementation strength of carbonate is greater than that of clay and gravels are less likely to be destroyed at the edge of the matrix.

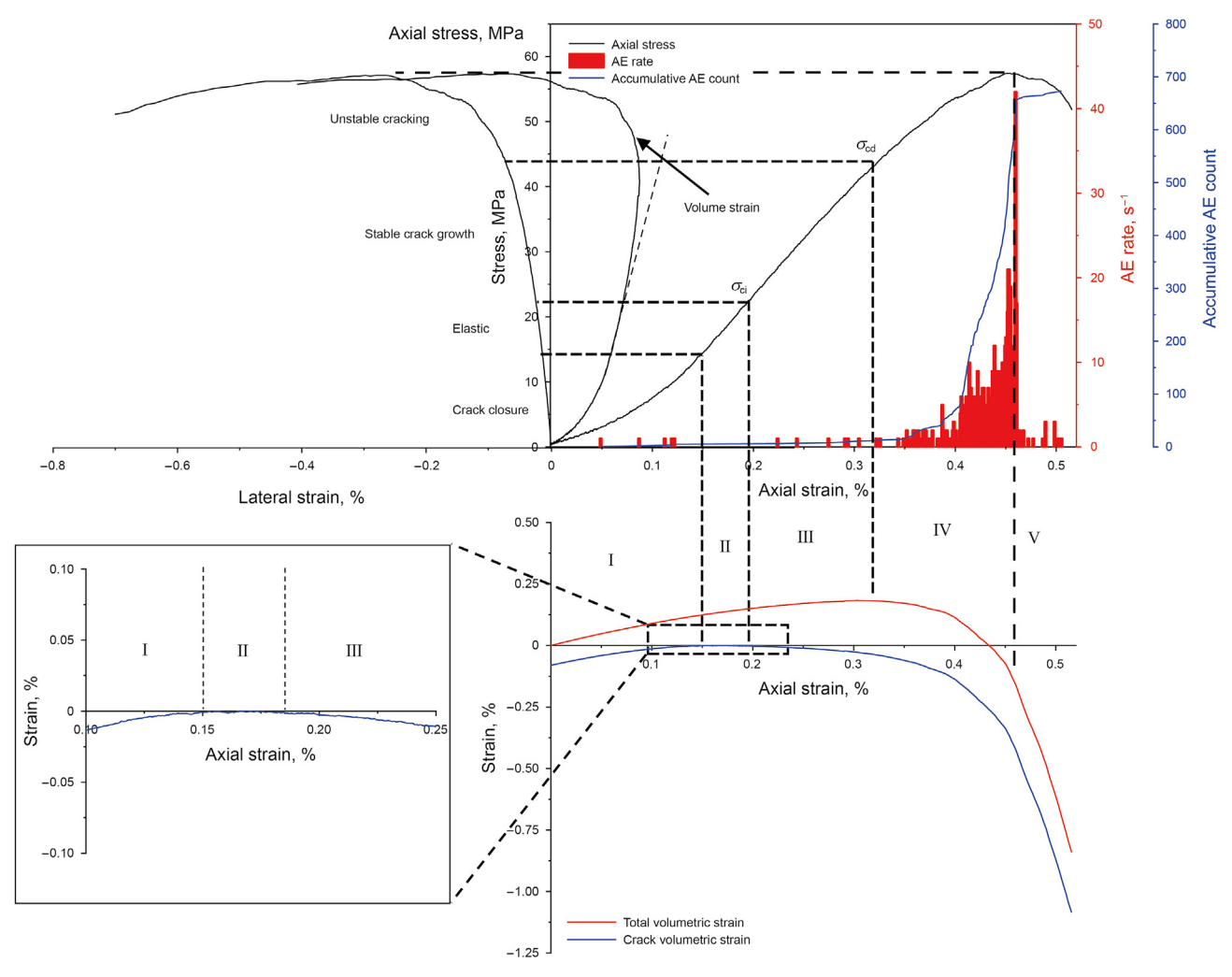


Fig. 12. Stress-strain diagram showing the crack evaluation stages of specimen X1.

Fig. 15(b) shows the relationship between Poisson's ratio and gravel content. When the carbonate cemented conglomerate has a gravel content of 25.5 vol%, Poisson's ratio is 0.17, and when the gravel content increases to 41.2 vol%, Poisson's ratio increases to 0.24. However, as the gravel content further increases to 60.3 vol%, Poisson's ratio decreases to 0.09. In the case where the clay cemented conglomerate has a gravel content of 10.4 vol%, Poisson's ratio is 0.17. With the increase of gravel content, Poisson's ratio gradually decreases, and when the gravel content is 63.3 vol%, Poisson's ratio is 0.48. Poisson's ratio of carbonate cemented conglomerate specimens increases first and then decreases with the increase of gravel content. But for clay cemented conglomerate specimens, their Poisson's ratio solely increases with the increase of gravel content. Poisson's ratio of rock reflects the deformation characteristics of rock under stress. The bigger Poisson's ratio is, the softer the rock is and the larger the plasticity of rock is. The rock with smaller Poisson's ratio is hard and brittle (Zhang et al., 2011). Poisson's ratio is the basic property of rock, which is related to the mineral composition and the mineral content of the rock. For conglomerate, Poisson's ratio is controlled by the mechanical properties and the content of the constituent phases. However, the research related to this issue is deficient at present.

4.2. Influencing factors of fracture morphology and formation mechanism

4.2.1. Factors influencing fracture complexity

The fractal dimension and intersection index of carbonate cemented conglomerate and clay cemented conglomerate vary with gravel content as shown in Fig. 16. Fig. 16(a) shows the curve of fractal dimension of carbonate cemented conglomerate versus gravel content. It can be seen that the fractal dimension increases from 2.097 to 2.295 as the gravel content increase from 25.5 to 41.2 vol% and then decreases from 2.295 to 2.175 with gravel content ranging from 41.2 to 60.3 vol%.

The variation curve of the intersection index of carbonate cemented conglomerate versus gravel content is given in Fig. 16(b). It can be seen that the intersection index increases from 4.51 to 10.5 as the gravel content increase from 25.5 to 41.2 vol%, and then decreases from 10.5 to 5.33 with the gravel content increasing from 41.2 to 60.3 vol%. By considering the fracture morphology (Fig. 9) of carbonate cemented conglomerate combined with its fracture tortuosity and distribution density, it can be seen that for carbonate cemented conglomerate with low gravel content, the fractures are simple ones with low tortuosity and distribution density that

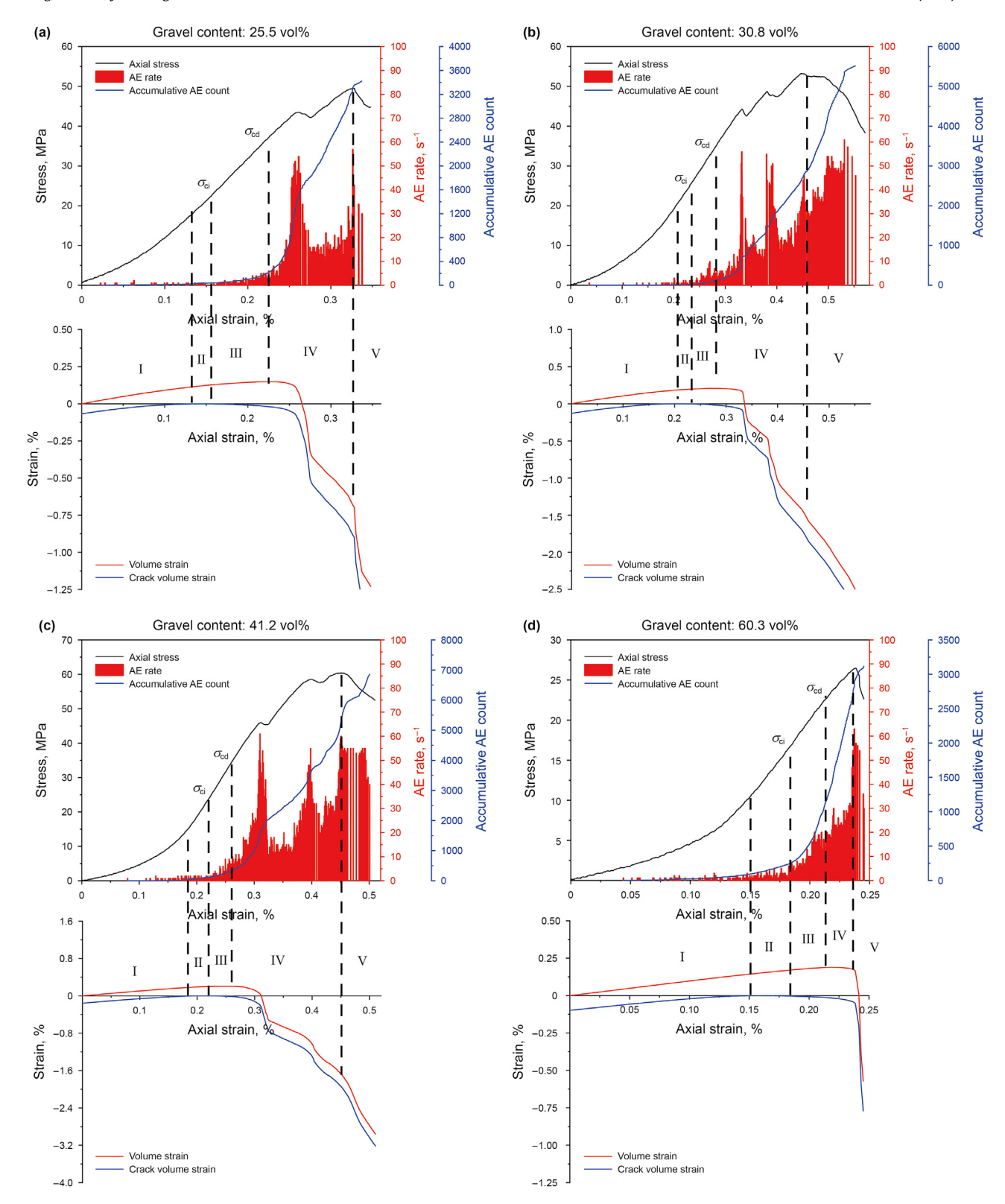


Fig. 13. Stress-strain diagram showing the crack evaluation stages of specimens from group Z.

surround gravels. With the increase of gravel content, the fractures are more and more complex. When gravel content is 41.2 vol%, the fractures manifest as the complex fracture network developed by both gravel-surrounding and gravel-penetrating fractures, with high tortuosity and high distribution density. When the gravel

content exceeds 41.2 vol%, the fracture tortuosity decreases, and the distribution density decreases with gravel content increasing. When the gravel content is 60 vol%, fractures are simple gravel-penetrating fractures. Fig. 16(c) shows the variation curve of fractal dimension of clay cemented conglomerate specimens versus

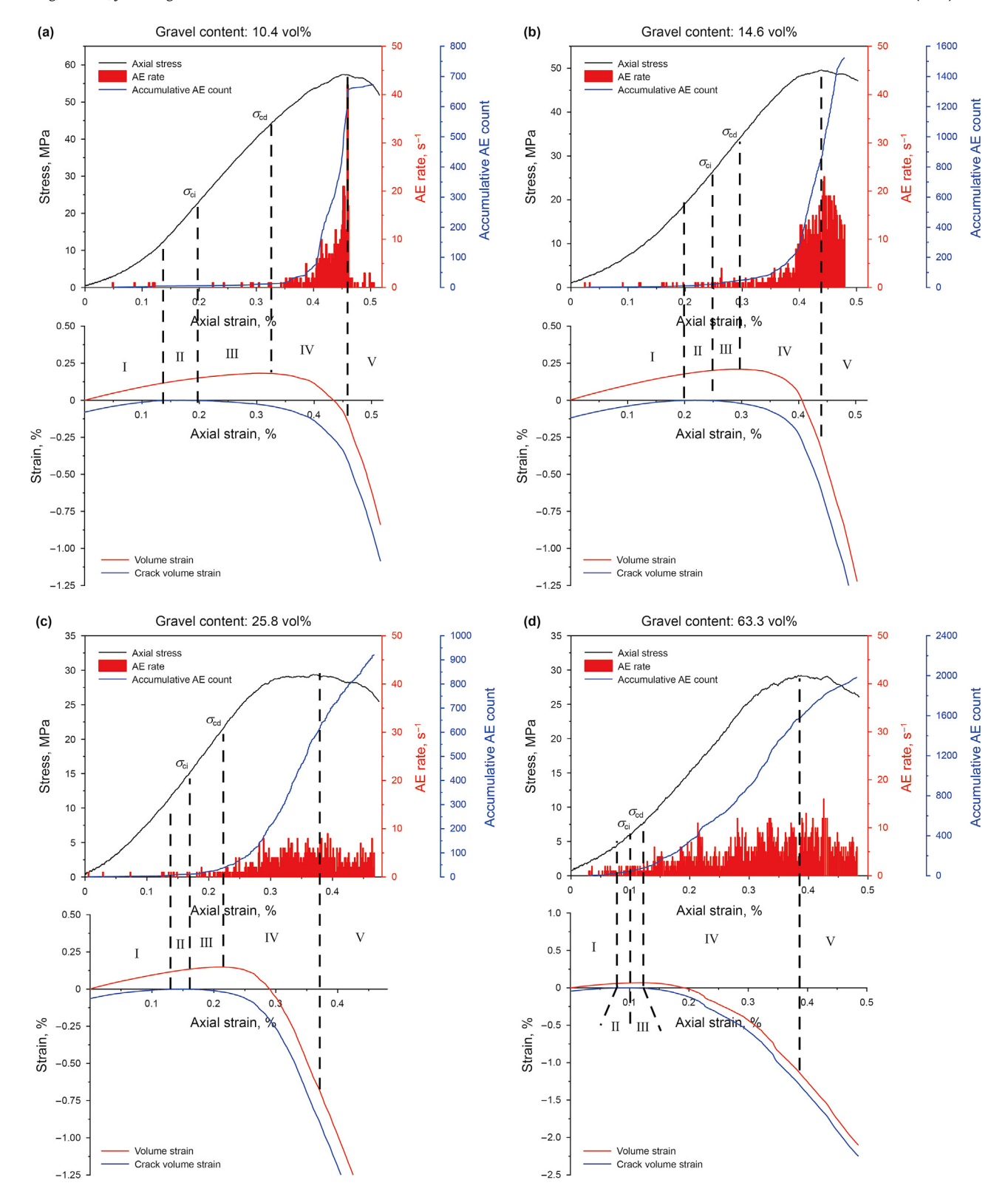


Fig. 14. Stress—strain diagram showing the stages of crack evaluation of specimens from group X.

gravel content. It can be seen that the fractal dimension increases from 2.20 to 2.13 as the gravel content decrease from 10.4 to 35.6 vol%, and then increases from 2.13 to 2.36 with the gravel content increasing from 35.6 to 63.3 vol%. Fig. 16(d) shows the variation curve of the intersection index of clay cemented

conglomerate specimens versus gravel content. It is clear that the intersection index increases from 3.50 to 11.6 with the gravel content increasing from 10.4 to 63.3 vol%. Thus, it can be concluded that the fracture complexity of clay cemented conglomerate specimens increases with the increase of gravel content.

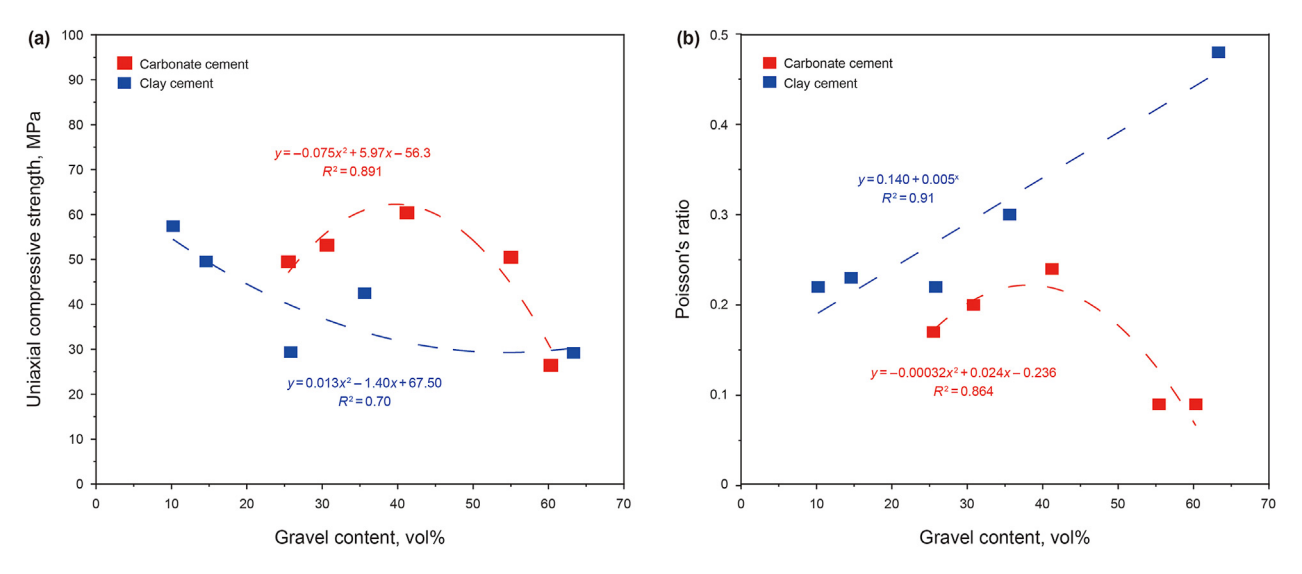


Fig. 15. Relationship curve between mechanical properties of conglomerate and gravel content.

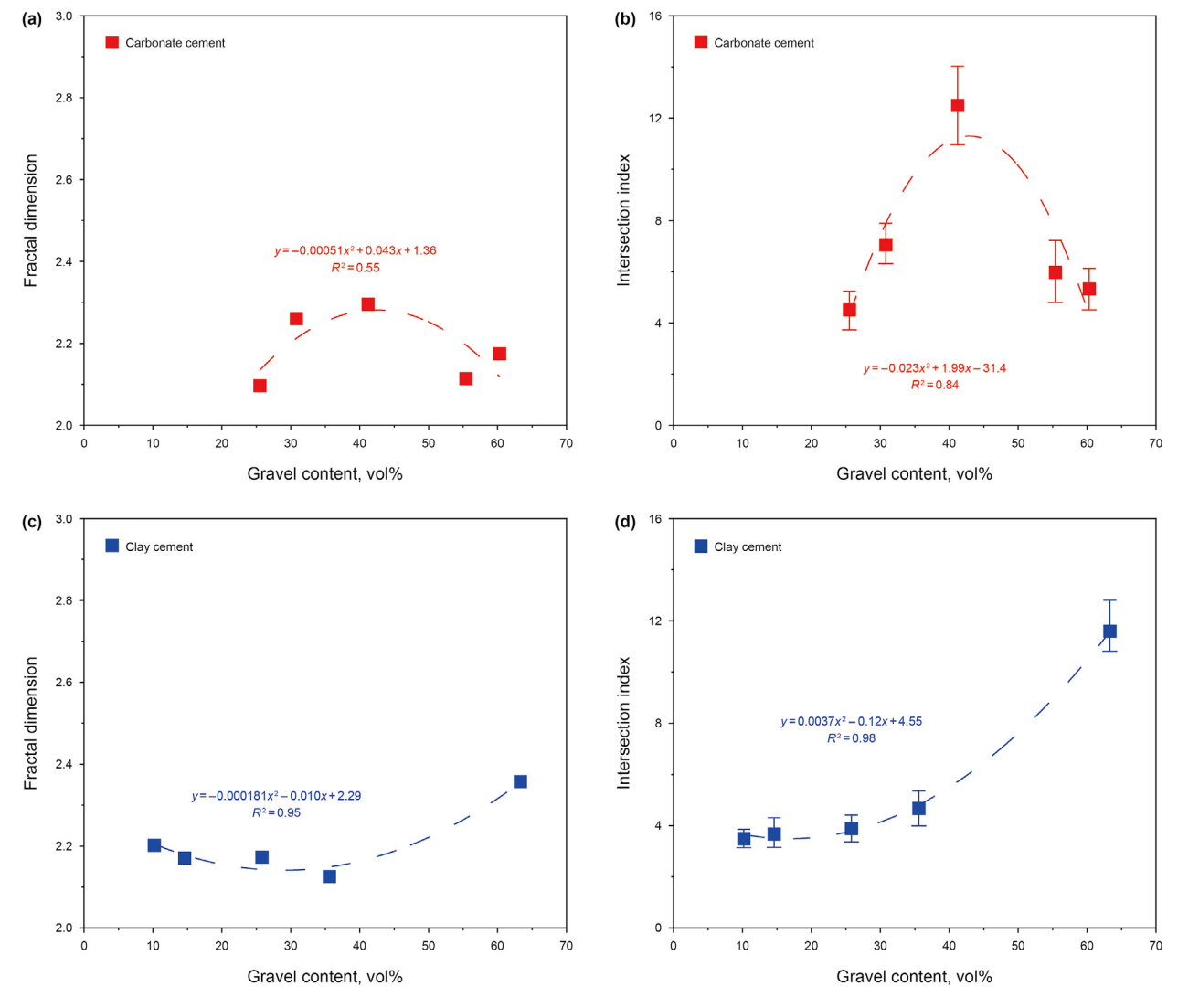


Fig. 16. The influence of gravel content on fractal dimension and intersection index.

The complexity of carbonate cemented conglomerate fractures varies with the gravel content, and there is an inflection point at the gravel content of about 40 vol%, which is consistent with the phenomenon observed in the previous numerical simulation study of conglomerate fracturing (Luo et al., 2021). There are two reasons for the fractures of conglomerate under the action of stress. (1) According to the Mohr—Coulomb failure criterion (Labuz and Zang. 2012), under the action of stress, the rock will undergo shear failure along a fracture plane, forming a shear fracture. (2) Due to the large difference in mechanical properties between gravels and the matrix (Li et al., 2022), the strains of the gravels and the matrix are not coordinated under stress, and fractures are generated at the cementation of the gravels and the matrix. When the gravel content is 0–20 vol%, the gravels are wrapped by the matrix, there is little or no contact between gravels, and the matrix bears the main stress. Under the action of stress, the conglomerate will undergo shear failure along a fracture plane, forming a shear fracture. Since the gravel content is small, fractures at the cementation of the gravels and the matrix are difficult to coalesce with each other and expand, and thus the overall fracture morphology of the conglomerate is simple (for example, sample X1, Fig. 10 and sample Z1, Fig. 9). When the gravel content is 20–40 vol%, more gravels are prone to contact with each other, and the factures at the cementation of the gravels and the matrix will expand around the gravel and through the gravel (Liu et al., 2016). With the increase of the gravel content, a large number of fractures that are around the gravel and through the gravel will occur, and the tortuosity and distribution density of the fractures will also increase. When the gravel content is larger than 40 vol%, the gravels contact with each other and bear the main stress. In this case, the elastic modulus of gravels is greater than that of the matrix (Li et al., 2022), and the elastic strain of the conglomerate before fracturing is less than that in the case of 0-20 vol% of gravel content (X1 is 0.26%, X5 is 0.15%; Z1 is 0.21%, Z5 is 0.20%). Therefore, the fractures at the cementation of the gravels and the matrix are not prone to be formed. Since the carbonate has a high cementation strength, the fractures at the cementation of the gravels and the matrix are not prone to be formed either, which leads to the simple morphology of fractures, as shown by sample Z5.

4.2.2. Influencing factors of crack evolution

From the study of crack evolution of homogeneous rocks such as sandstone and granite, the following conclusions can be drawn from data analysis. (1) Crack initiation stress $\sigma_{\rm ci}$ is about 0.3–0.5 times of peak stress, and (2) crack propagation stress $\sigma_{\rm cd}$ is approximately 0.7–1.0 times of peak stress (Brace et al., 1966; Martin, 1993; Eberhardt et al., 1999; Hatzor and Palchik, 1997). In this study, it has been observed that the initiation stress of cracks $\sigma_{\rm ci}$ in the conglomerate specimen is approximately 0.25–0.50 times of peak stress $\sigma_{\rm f}$, which is similar to previous studies of homogeneous rocks. The crack development stress $\sigma_{\rm cd}$ is about 0.25–0.90 times of peak stress $\sigma_{\rm f}$, which is quite different from that of homogeneous rock.

Fig. 17 shows the relationship of $\sigma_{\rm ci}/\sigma_{\rm f}$ and $\sigma_{\rm cd}/\sigma_{\rm f}$ versus gravel content. It can be seen that there is no obvious correlation between gravel content and $\sigma_{\rm ci}/\sigma_{\rm f}$, as shown in Fig. 17(a). On the contrary, $\sigma_{\rm cd}/\sigma_{\rm f}$ has a strong correlation with gravel content, and the relationship curves of conglomerate with different cementation types are different, as shown in Fig. 17(b). The percentage of crack development stress of carbonate cemented conglomerate decreases first and then increases with gravel content. While the percentage of crack propagation stress of clay cemented conglomerate decreases with the increase in gravel content. The size of the percentage of crack development stress represents the sooner or later when the crack develops. The larger the percentage is, the later the crack develops,

the shorter the time for development is, and the smaller the fracture process zone is. Conversely, the smaller the percentage is, the earlier the crack develops, the longer the time for development is, and the larger the fracture process zone is. For both the carbonate cemented conglomerates and the clay cemented conglomerates, when the gravel content is in a range of 0-40 vol%, the percentage of crack development stage and the fracture process zone become larger with the increase in gravel content. This is because that the stress concentration is prone to appear at the interface of gravels and matrix due to the strain incompatibility and the strength of the interface is low, so the interface area starts to fracture first. With the increase of the gravel content, the interface area between gravels and matrix also increases, which makes the interface crack earlier, thus increasing the percentage of the crack development stage. When the gravel content is greater than 40 vol%, the percentage of crack development stage of carbonate cemented conglomerate decreases with the increase of gravel content. This is because when the gravel content exceeds 40 vol%, the gravels in the conglomerate contact with each other, and the support mode becomes gravel-supported, making gravels bearing a larger stress. The interface area of carbonate cemented conglomerate has a relatively high cementation strength, so it is less likely to form fractures, and the percentage of crack development stage is thus reduced. However, clay cemented conglomerate is more prone to fracture due to its low cementation strength, and the percentage of crack development stage increases.

Fig. 18 shows the relationship between the percentage of crack development stress ($\sigma_{\rm cd}/\sigma_{\rm f}$) and the intersection index. It can be seen that the percentage of crack development stress is negatively correlated with the intersection index, indicating that the earlier the crack develops, the more branch fractures are eventually formed.

Based on the above analysis, it is believed that the crack evolution and fracture morphology characteristics of the conglomerate are affected by both gravel content and cementation types of the conglomerate, as shown in Fig. 19. When the gravel content is relatively low, the carbonate cemented conglomerate and clay cemented conglomerate have similar properties. Specifically, the crack develops late, the fracture process zone is small, and the fracture morphology form is simple. With the increase of gravel content, the crack development stress decreases, the fracture process zone increases, and the fracture morphology becomes more and more complex. In the carbonate cemented conglomerate, the gravel-surrounding fractures and gravel-penetrating fractures are developed together. In the clay cemented conglomerate, the gravelsurrounding fractures are mainly, but the gravel-penetrating fractures are seldom formed. When the gravel content reaches the level that gravel support can be formed, with the gravel content increasing continually, the crack development stress of carbonate cemented conglomerate increases, forming simple gravelpenetrating fractures. While for clay cemented conglomerate, the crack development stress continues to decrease, forming a complex fracture network jointly developed by gravel-surrounding fractures and gravel-penetrating fractures.

4.3. Uncertainty analysis and research suggestions

In this article, the uniaxial compression test, acoustic emission monitoring, and CT scanning are used to study the fracturing process and fracture morphology characteristics of conglomerate. According to different cementation types, the conglomerate can be divided into carbonate cemented conglomerate and clay cemented conglomerate. The relationship between the fracturing characteristics and fracture morphology and the gravel content and cementation type of these two types of conglomerate is studied respectively. Nevertheless, the methods used in this article have

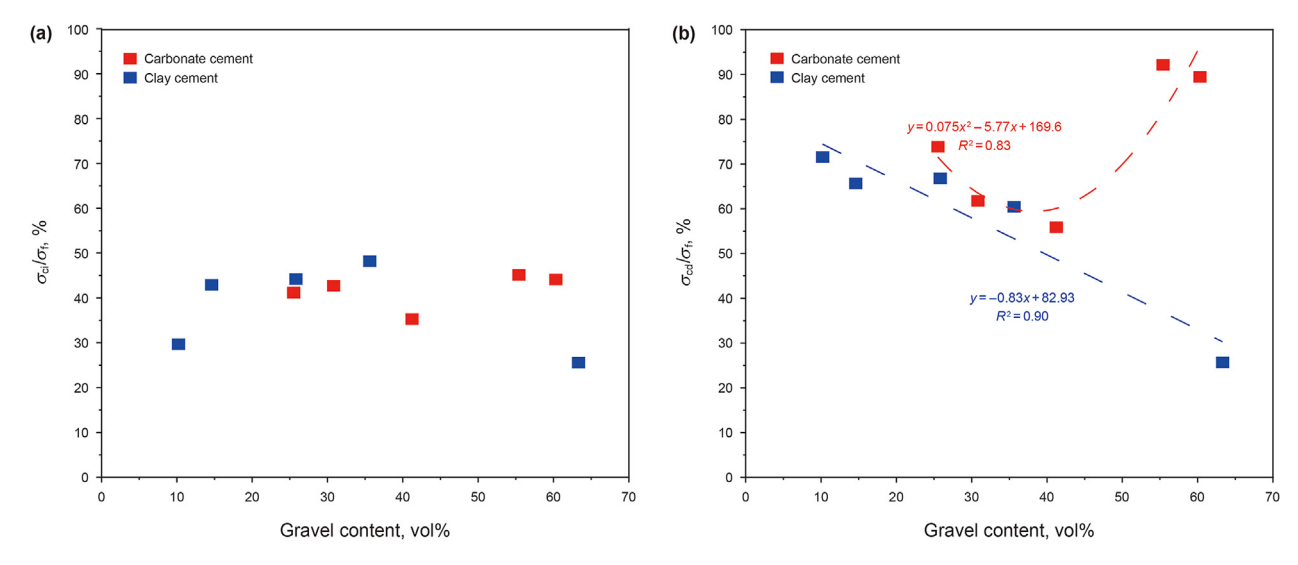


Fig. 17. The influence of gravel content on $\sigma_{\rm ci}/\sigma_{\rm f}$ and $\sigma_{\rm cd}/\sigma_{\rm f}$.

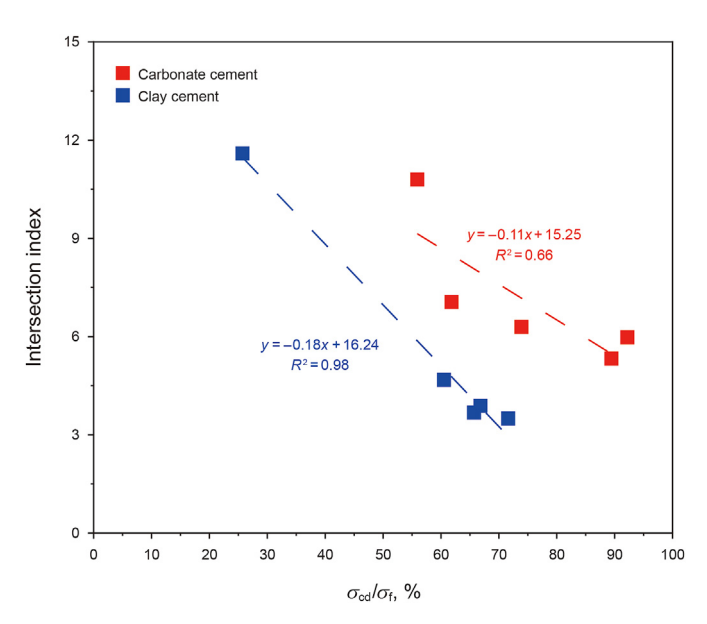


Fig. 18. Relationship curve between intersection index and σ_{cd}/σ_f .

some limitations:

- (1) When the fracture distribution density of the conglomerate is analyzed by the Sholl method, the statistical data are processed by two average treatments. The first is to average the number of the intersection point of each ring and fractures in each CT image. The variance of the geometric mean, the arithmetic mean, the median and the mode is calculated, respectively, and the arithmetic mean is chosen as the mean value for additional processing and analysis. The second average treatment is to further average the number of the intersection points in the 10 images for each sample. In addition, an error bar is used to identify the 95% confidence interval in the graph (Fig. 16).
- (2) The conglomerate sample used in this article is 38 mm in diameter and 76 mm in height, which is sufficient for studying gravels with smaller diameter. However, it has been noticed that gravels in some formations of Mahu sag have a

- diameter of more than 50 mm, and it is difficult to study the fracturing characteristics of such large-scale conglomerate through traditional laboratory tests.
- (3) In this study, instead of scanning all areas of the sample, the middle part of the sample is subjected to CT scanning. This is mainly to meet the requirements for CT image resolution. In order to recognize the micro fractures more clearly and make the scanning area larger as much as possible, the resolution is determined to be 15 μm after several tests and adjustments. Meanwhile, the scanning area is in the middle of the sample, thus avoiding the impact of fractures on the end face of the sample caused by stress concentration on the test results. However, this method is only an alternative one, and there are still some fractures that have not been scanned. In subsequent experiments, better test equipment should be used to scan the test samples in a full range.
- (4) The conglomerate strength in this study is mostly qualitatively described, lacking quantitative characterization of the properties of each component of conglomerate. In the following research, it is suggested that the micromechanical test means should be used to measure the mechanical properties of each constituent of conglomerate and analyze the characteristics of conglomerate fracturing and the fractures formed.

5. Conclusions

In this study, uniaxial compression, acoustic emission monitoring, and CT scanning were used to investigate the fracture characteristics of the conglomerate and their controlling factors, especially the cementation type and gravel content. The following conclusions may be drawn:

- According to the stress—strain curves and AE characteristics, the fracture characteristics of the conglomerate are complex and are affected by the cementation type and the gravel content.
- (2) The mechanical properties of conglomerates are affected by the gravel content and the cement. The compressive strength of conglomerate decreases with the increase of gravel content. When the gravel content is the same, the compressive

Gravel content, vol%		20	40	60
Support pattern		Matrix support	Matrix and gravel support	Gravel support
Carbonate cemented conglomerate	Fracture shapes			
	Fracture morphology characteristics	The single fracture characterized by deflection	The complicated fracture characterized by deflection and penetration	The single fracture characterized by penetration
	Intersection index	4.1	10.5	4.2
	σ _{cd} /σ _f , %	73.9	55.9	89.4
Clay cemented conglomerate	Fracture shapes			
	Fracture morphology characteristics	The single fracture characterized by deflection	The complicated fracture characterized by deflection	The complicated fracture characterized by deflection
	Intersection index	3.9	7.4	11.5
	$\sigma_{ m cd}/\sigma_{ m f},\%$	71.6	60.5	25.7

Fig. 19. Conglomerates classification according to the gravel content and the cement.

- strength of carbonate cemented conglomerate is greater than that of clay cemented conglomerate.
- (3) The crack evolution process of the conglomerate can be divided into five stages. The crack development stress is a significant parameter in the crack evaluation of conglomerates.
- (4) The conglomerate can be divided into carbonate cemented conglomerate and clay cemented conglomerate, according to the composition of the cement. The fracture morphology, complexity, and regularity of these two types of conglomerates are different.
- (5) For carbonate cemented conglomerates, the relationship between fracture characteristics and gravel content shows two change stages. (a) With the gravel content increasing from about 25 to 40 vol%, the crack development stress decreases, and fractal dimension and intersection index increase. The increase in fracture complexity is accompanied by the fracture morphology changing from simple gravel-surrounding fractures to a fracture network developed by both gravel-surrounding and gravel-penetrating fractures. (b) With the gravel content increasing from about 40 to 60 vol%, the crack development stress increases, and fractal
- dimension and intersection index decrease. The fracture complexity is reduced and the fracture morphology changes from a fracture network developed by both gravel-surrounding and gravel-penetrating fractures to a simple gravel-penetrating fracture.
- (6) For clay cemented conglomerates, the crack development stress decreases and the fractal dimension and intersection index increase with increasing gravel content. The fracture complexity increases and the fracture morphology changes from a simple gravel-surrounding fracture to a fracture network developed by both gravel-surrounding and gravelpenetrating fractures.

Declaration of competing interest

The authors declare that they have no known competing financial interests or personal relationships that could have appeared to influence the work reported in this paper.

Acknowledgements

This work was supported by the Natural Science Youth Project of

University Scientific Research Plan in Xinjiang (XJEDU2021Y053), the Talent Introduction Research Project of China University of Petroleum Beijing at Karamay (XQSQ20200056), Development of Conglomerate Reservoir Laboratory in Xinjiang (2019D04008), the Strategic Cooperation Technology Projects of CNPC and CUPB (Grant No. ZLZX2020-01).

References

- Abdelaziz, A., Zhao, Q., Grasselli, G., 2018. Grain based modelling of rocks using the combined finite-discrete element method. Comput. Geotech. 103, 73–81. https://doi.org/10.1016/j.compgeo.2018.07.003.
- Arnott, R.W.C., 2003. The role of fluid- and sediment-gravity flow processes during deposition of deltaic conglomerates (Cardium Formation, Upper Cretaceous), West-Central Alberta. Bull. Can. Petrol. Geol. 51 (4), 426–436. https://doi.org/ 10.2113/51.4.426.
- Brace, W.F., Paulding Jr., B.W., Scholz, C., 1966. Dilatancy in the fracture of crystalline rocks. J. Geophys. Res. 71 (16), 3939–3953. https://doi.org/10.1029/JZ071i016p03939.
- Cnudde, V., Boone, M., Dewanckele, J., et al., 2011. 3D characterization of sandstone by means of X-ray computed tomography. Geosphere 7 (1), 54–61. https:// doi.org/10.1130/GES00563.1.
- Cronin, B.T., Kidd, R.B., 1998. Heterogeneity and lithotype distribution in ancient deep-sea canyons: point Lobos deep-sea canyon as a reservoir analogue. Sediment. Geol. 115 (1/2/3/4), 315–349. https://doi.org/10.1016/S0037-0738/97/00099-7.
- Eberhardt, E., Stead, D., Stimpson, B., 1999. Quantifying progressive pre-peak brittle fracture damage in rock during uniaxial compression. Int. J. Rock Mech. Min. Sci. 36 (3), 361–380. https://doi.org/10.1016/S0148-9062(99)00019-4.
- Erarslan, N., 2013. A study on the evaluation of the fracture process zone in CCNBD rock samples. Exp. Mech. 53 (8), 1475–1489. https://doi.org/10.1007/s11340-013-9750-5
- Falconer, K., 2014. Fractal Geometry: Mathematical Foundations and Applications, Third ed. John Wiley & Sons Ltd, ISBN 978-1-119-94239-9.
- Ferreira, T., Blackman, A., Oyrer, J., et al., 2014. Neuronal morphometry directly from bitmap images. Nat. Methods 11 (10), 982–984. https://doi.org/10.1038/nmeth 3125
- Griffith, A.A., 1921. The phenomena of rupture and flow in solids. Philos. Trans. R. Soc. A Math. Phys. Eng. Sci. A221 (4), 163–198. https://doi.org/10.1098/rsta1921.0006
- Hatzor, Y.H., Palchik, V., 1997. The influence of grain size and porosity on crack initiation stress and critical flaw length in dolomites. Int. J. Rock Mech. Min. Sci. 3 4 (5), 805–816. https://doi.org/10.1016/S1365-1609(96)00066-6.
- He, X., Ma, J., Liu, G., et al., 2019. Analysis of rock mechanics and assessments of hydraulic fracture network in conglomerate reservoirs of Mahu oilfield. Xinjing Pet. Geol. 40 (6), 701–707 (in Chinese).
- Hentz, T.F., Ambrose, W.A., Carr, D.L., 2012. Reservoir systems of the pennsylvanian lower atoka group (bend conglomerate), northern fort worth basin, Texas: highresolution facies distribution, structural controls on sedimentation, and production trends. AAPG (Am. Assoc. Pet. Geol.) Bull. 96 (7), 1301–1332. https:// doi.org/10.1306/10041111078.
- Hou, Q., He, H., Li, J., Yang, T., 2018. Recent progress and prospect of oil and gas exploration by PetroChina Company Limited. China Petrol. Explor. 23 (1), 1–13. https://doi.org/10.3969/j.issn.1672-7703.2018.01.001 (in Chinese).
- Janeiro, R.P., Einstein, H.H., 2010. Experimental study of the cracking behavior of specimens containing inclusions (under uniaxial compression). Int. J. Fract. 164, 83–102. https://doi.org/10.1007/s10704-010-9457-x.
- Jia, C., Zou, C., Yang, Z., et al., 2018. Significant progress of continental petroleum geological theory in basins of Central and Western China. Petrol. Explor. Dev. 45 (4), 573–588. https://doi.org/10.1016/S1876-3804(18)30064-8.
- Jia, H., Ji, H., Wang, L., et al., 2017. Reservoir quality variations within a conglomeratic fan-delta system in the Mahu sag, northwestern Junggar Basin: characteristics and controlling factors. J. Petrol. Sci. Eng. 152, 165–181. https://doi.org/ 10.1016/j.petrol.2017.03.002.
- Jia, L., Chen, M., Zhang, W., et al., 2013. Experimental study and numerical modeling of brittle fracture of carbonate rock under uniaxial compression. Mech. Res. Commun. 50, 58–62. https://doi.org/10.1016/j.mechrescom.2013.04.002.
- Ju, Y., Zheng, J., Epstein, M., et al., 2014. 3D numerical reconstruction of well-connected porous structure of rock using fractal algorithms. Comput. Methods Appl. Mech. Eng. 279, 212–226. https://doi.org/10.1016/j.cma.2014.06.035.
- Labuz, J.F., Zang, A., 2012. Mohr-Coulomb failure criterion. Rock Mech. Rock Eng. 45, 975–979. https://doi.org/10.1007/s00603-012-0281-7.
- Li, J., Duan, K., Meng, H., et al., 2022. On the Mechanical properties and failure mechanism of conglomerate specimens subjected to triaxial compression tests. Rock Mech. Rock Eng. 56, 973—995. https://doi.org/10.1007/s00603-022-03110-4
- Li, L., Meng, Q., Wang, S., et al., 2013. A numerical investigation of the hydraulic fracturing behaviour of conglomerate in Glutenite formation. Acta Geotech. 8 (6), 597–618. https://doi.org/10.1007/s11440-013-0209-8.

- Liu, J., Ge, H., Zhang, Z., et al., 2022. Influence of mechanical contrast between the matrix and gravel on fracture propagation of glutenite. J. Petrol. Sci. Eng. 208 (C), 109639. https://doi.org/10.1016/j.petrol.2021.109639.
- Liu, P., Ju, Y., Ranjith, P.G., et al., 2016. Experimental investigation of the effects of heterogeneity and geostress difference on the 3D growth and distribution of hydrofracturing cracks in unconventional reservoir rocks. J. Nat. Gas Sci. Eng. 35, 541–554. https://doi.org/10.1016/j.jingse.2016.08.071.
- Liu, X., Xiong, J., Liang, L., et al., 2018. Rock Mechanical characteristics and fracture propagation mechanism of sandy conglomerate reservoirs in Baikouquan Formation of Mahu Sag. Xinjing Pet. Geol. 39 (1), 83–91. https://doi.org/10.7657/ XIPG20180108 (in Chinese).
- Luo, S., Ge, H., Wang, J., et al., 2021. Numerical simulation study on the crack propagation of conglomerate. R. Soc. Open Sci. 8 (7), 202178. https://doi.org/10.1098/rsos.202178
- Ma, D., Luo, Y., Hu, D., et al., 2020. Effects of particle size sorting and confining pressure on hydraulic fracturing mechanism of glutenite rock. Chin. J. Rock Mech. Eng. 39 (11), 2264–2273. https://doi.org/10.13722/j.cnki.jrme.2020.0006 (in Chinese).
- Ma, X., Zou, Y., Li, N., et al., 2017. Experimental study on the mechanism of hydraulic fracture growth in a glutenite reservoir. J. Struct. Geol. 97, 37–47. https:// doi.org/10.1016/j.jsg.2017.02.012.
- MacQuaker, J.H.S., Taylor, K.G., Keller, M., et al., 2014. Compositional controls on early diagenetic pathways in fine-grained sedimentary rocks: implications for predicting unconventional reservoir attributes of mudstones. AAPG (Am. Assoc. Pet. Geol.) Bull. 98 (3), 587–603. https://doi.org/10.1306/08201311176.
- Martin, C.D., 1993. The Strength of Massive Lac du Bonnet Granite Around Underground Openings. Doctoral dissertation. University of Manitoba (Canada).
- Martin, C.D., Chandler, N.A., 1994. The progressive fracture of Lac du Bonnet granite. Int. J. Rock Mech. Min. Sci. Geomech. Abstracts 31 (6), 643–659. https://doi.org/10.1016/0148-9062(94)90005-1.
- Meng, Q., Zhang, S., Guo, X., et al., 2010. A primary investigation on propagation mechanism for hydraulic fracture in glutenite formation. J. Oil Gas Technol. (J. Jianghan Petroleum Inst.) 32 (4), 119–123 (in Chinese).
- Peitgen, H.O., Jürgens, H., Saupe, D., 2004. Chaos and Fractals: New Frontiers of Science. Springer Science & Business Media.
- Pestman, B.J., van Munster, J.G., 1996. An acoustic emission study of damage development and stress-memory effects in sandstone. Int. J. Rock Mech. Min. Sci. Geomech. Abstracts 33 (6), 585–593. https://doi.org/10.1016/0148-9062(96)00011-3.
- Rui, Z., Guo, T., Feng, Q., et al., 2018. Influence of gravel on the propagation pattern of hydraulic fracture in the glutenite reservoir. J. Petrol. Sci. Eng. 165, 627–639. https://doi.org/10.1016/j.petrol.2018.02.067.
- Scholz, C.H., 1968. Experimental study of the fracturing process in brittle rock. J. Geophys. Res. 73 (4), 1447–1454. https://doi.org/10.1029/JB073i004p01447.
- Sholl, D.A., 1953. Dendritic organization in the neurons of the visual and motor cortices of the cat. J. Anat. 87 (4), 387–406.
- Tapponnier, P., Brace, W.F., 1976. Development of stress-induced microcracks in Westerly granite. Int. J. Rock Mech. Min. Sci. Geomech. Abstracts 13 (4), 103–112. https://doi.org/10.1016/0148-9062(76)91937-9.
- Tatone, B.S.A., Grasselli, G., 2015. Characterization of the effect of normal load on the discontinuity morphology in direct shear specimens using X-ray micro-CT. Acta Geotech. 10, 31–54. https://doi.org/10.1007/s11440-014-0320-5.
- Wang, J., Fu, J., Song, W., et al., 2021a. Acoustic emission characteristics and damage evolution process of layered cemented tailings backfill under uniaxial compression. Construct. Build. Mater. 295, 123663. https://doi.org/10.1016/ j.conbuildmat.2021.123663.
- Wang, J., Zhou, L., Jin, J., et al., 2021b. Characteristics of high-quality glutenite reservoirs of urho Formation in manan area, Junggar Basin. Lithol. Reserv. 33 (5), 34–44. https://doi.org/10.12108/yxyqc.20210504 (in Chinese).
- Wawersik, W.R., Brace, W.F., 1971. Post-failure behavior of a granite and diabase. Rock Mech. 3 (2), 61–85. https://doi.org/10.1007/BF01239627.
- Xi, K., Cao, Y., Haile, B.G., et al., 2021. Diagenetic variations with respect to sediment composition and paleo-fluids evolution in conglomerate reservoirs: a case study of the Triassic Baikouquan Formation in Mahu Sag, Junggar Basin, Northwestern China. J. Petrol. Sci. Eng. 197, 107943. https://doi.org/10.1016/ j.petrol.2020.107943.
- Xv, C., Zhang, G., Yanjun, L., et al., 2019. Experimental study on hydraulic fracture propagation in conglomerate reservoirs. In: 53rd US Rock Mechanics Geomechanics Symposium.
- Zhang, N., Sheng, Z., Li, X., et al., 2011. Study on the relationship between Poisson's ratio and internal friction Angle of rock. Chin. J. Rock Mech. Eng. S1, 2599—2609 (in Chinese).
- Zhang, Y., Niu, S., Du, Z., et al., 2020. Dynamic fracture evolution of tight sandstone under uniaxial compression in high resolution 3D X-ray microscopy. J. Petrol. Sci. Eng. 195, 107585. https://doi.org/10.1016/j.petrol.2020.107585.
- Zhu, J., Qiao, C., Song, Y., et al., 2019. Effect of particle characteristics on shear strength of weakly cemented conglomerate in tertiary. J. Harbin Inst. Technol. 51 (5), 100–109 (in Chinese).
- Zhu, N., Cao, Y., Xi, K., et al., 2019. Diagenesis and physical properties evolution of sandy conglomerate reservoirs: a case study of Triassic Baikouquan Formation in northern slope zone of Mahu Depression. J. China Inst. Min. Technol. 48, 1102–1118 (in Chinese).